Elastodiffusion calculation of asymptotic absorption efficiences and bias factors of dislocations in Al, Ni and Fe

Liangzhao Huang, Maylise Nastar, Luca Messina, Thomas Schuler

Elastodiffusion calculation of asymptotic absorption efficiencies and bias factors of dislocations in Al, Ni and Fe

Liangzhao Huang[a,b,*], Maylise Nastar[a], Luca Messina[c], Thomas Schuler[a]

[a] *Université Paris-Saclay, CEA, Service de Recherches de Métallurgie Physique, 91191, Gif-sur-Yvette, France*
[b] *Aix Marseille Université, CNRS, IM2NP, Marseille, France*
[c] *CEA, DEs, IRESNE, DEC-Service d'Études et de Simulation du Comportement des Combustibles, Cadarache F-13108 Saint-Paul-Lez-Durance, France*

Abstract

The elastic interactions between dislocations and lattice point defects (PDs) control the rate of PD elimination at dislocations, and thereby the PD spatial distribution within the microstructure. By relying on the Onsager formalism, we introduce a new partition of the PD diffusion driving force in a strain field. We present DFT-based calculations of straight and loop-form edge dislocation absorption efficiencies and the resulting biases of vacancy and self-interstitial elimination in pure Fe, Ni, and Al metals. We highlight the effects of the dislocation density, the temperature and the dislocation orientation on the elastodiffusion behavior and the resulting PD redistribution near dislocations. Based on a detailed study of the sensitivity of absorption efficiencies to the boundary conditions, i.e., the capture radius and the associated PD concentrations, we introduce the notion of asymptotic absorption efficiencies and bias.

Keywords: Diffusion, Point defects, Elastic bias, Dislocation

1. Introduction

Microstructure evolution of materials under irradiation is a consequence of the transport of point defects (PDs). They are created in radiation–induced displacement cascades, then diffuse to eliminate at various PD sinks. Sinks can be structural extended pre-existing defects such as grain-boundaries, dislocation lines, surfaces, and PD clusters formed under irradiation such as dislocation loops or voids. These extended defects generate long-range stress-strain fields in the material, leading to long-range elastic interactions with the lattice PDs [1]. These elastic interactions modify the PD diffusion and elimination rate [1, 2, 3]. The specific action of the sink strain field on lattice PDs such as vacancies and self-interstitial atoms (SIA) leads to a sink bias, i.e., a preferential absorption of SIAs or vacancies. Each class of sink is typically assigned a partial sink strength with an absorption efficiency specific to each kind of PD, hence an absorption bias specific to each sink. Both the sink-dependent bias, and the difference of sink strengths between the different classes of sinks, are responsible for the partition of vacancy and SIAs elimination reactions that drive most of the microstructure changes. The preferential elimination of SIAs at dislocations leads to dislocation climb [1, 4]. Another by-product of the preferential absorption of SIA by dislocations is the formation of voids so that the overall elimination rate of PDs obeys a matter balance at steady state [5]. The formation of voids is the primary mechanism for swelling [5, 6]. Therefore, to understand radiation-induced phenomena, it is essential to obtain an estimation of the various sink biases.

Experimentally, the sink bias of a dislocation population is deduced from the measure of the growth rate of voids, or the macroscopic swelling rate of the irradiated sample. Unfortunately, this type of measurement is not very accurate. It is indeed difficult to extract a dislocation bias from experiments [7, 8], because the swelling rate is sensitive to the change of density and bias of all classes of sinks and to the fraction of mobile defects produced within cascades [9], which are not always precisely known.

A direct calculation of sink bias consists in solving the PD diffusion equation including the elastic drift force, and deducing the sink bias from the difference between the vacancy and interstitial fluxes towards the sink. It is now possible to compute a sink bias from DFT calculations of PD formation and migration energies, and PD elastic dipoles. From the elastic dipole formulation, one obtains the variation of jump frequencies with strain. The latter are then used as input parameters of either an object kinetic Monte Carlo method—to simulate and measure the PD flux towards ideal sinks, as for example in Al [10]—or a statistical physics diffusion method yielding the elastodiffusion driving forces and transport coefficients of a PD diffusion equation, which can be solved by means of a phase field method [11]. The PD diffusion driving force in a strain field was first given by Weertman [12] and later

*Corresponding author
Email addresses: huang.liangzhao@outlook.com (Liangzhao Huang), maylise.nastar@cea.fr (Maylise Nastar)

by Lothe and Hirth [4] from an analytical calculation of the vacancy chemical potential gradient. The first formulation of the PD diffusion coefficient including the elastic dipoles was from Dederichs [13]. Up to now, the chemical potential gradient of the substitutional atoms was missing in the derivations of the PD diffusion driving force. Yet, according to the thermodynamics of irreversible processes and its application to diffusion by Onsager, the flux of PD is a linear combination of both the PD and the atom chemical potential gradients [14, 15]. Surprisingly, the previous continuous diffusion methods, which were ignoring the variation of the atom chemical potential with strain, yielded PD absorption efficiencies very close to the exact direct Monte Carlo simulations [10, 11]. Furthermore, in both stochastic and continuous kinetic methods, diffusion in the close vicinity of sinks is not tackled, because near sinks such as dislocations, the lattice is strongly distorted. When the connectivity between lattice sites is partially lost, diffusion cannot be modeled as a series of on-lattice thermally activated events anymore. To overcome this technical difficulty, these methods systematically introduce a capture radius delimiting the surface across which PD jumps are treated as irreversible processes, as if PDs crossing the surface were instantaneously absorbed by the sink. Every study has its own justification for the chosen capture radius value, but very few of them have investigated the impact of their choice on PD absorption efficiencies.

The first aim of this work is to clarify the formulation of a diffusion-controlled phenomenon in a strain-stress heterogeneous field, in particular the PD and atom relative contributions to the diffusion driving force. Then, we investigate the impact of the boundary conditions at the capture radius on PD absorption efficiency and on the resulting bias. For this purpose, we rely on the general Onsager's expression of PD and atom fluxes, and deduce from it the PD diffusion coefficient and the diffusion driving force together with the elastic drift force. We apply it to a DFT-based calculation of straight and loop edge dislocations biases in Fe body-centered cubic (bcc) and Ni and Al face-centered cubic (fcc) metals. We first investigate the effects of temperature and dislocation density, and the less-known effect of the dislocation orientation on sink bias. A detailed sensitivity study is also performed to highlight the impact of the capture radius and the PD concentration at the capture radius on the absorption efficiencies of a dislocation line. Based on this sensitivity study, we introduce a method to deduce asymptotic values of the absorption efficiencies and the resulting bias.

This article is organized as follows. Section 2 is dedicated to the PD diffusion model. Then we present in Section 3 the simulation setup, the chosen boundary conditions, and the method to calculate the dislocation biases. Biases in Fe, Ni, and Al are calculated in Section 4 and we discuss the effects of dislocation density, temperature and dislocation orientations. Then the impact of the choice of capture radius and PD concentration at the capture radius is investigated in Section 5. Finally a summary, concluding remarks, and perspectives are given in Section 6.

2. Point-defect diffusion model

The absorption efficiency of a PD ($d \equiv$ I or V) on a given sink is obtained by calculating the flux of d towards the sink. The difference between the SIA and vacancy absorption efficiencies yields the sink bias. Following the Onsager's formalism [14, 16], we express the flux $\boldsymbol{J}_d$ of PD d in metal A and the flux $\boldsymbol{J}^d_{\mathrm{A}}$ of atom A mediated by d, as products of phenomenological transport coefficients and chemical potential gradients (CPG) acting as isothermal driving forces of diffusion,

$$\boldsymbol{J}_d = -\frac{1}{k_{\mathrm{B}}T}\left(\underline{L}_{dd}\boldsymbol{\nabla}\mu_d + \underline{L}_{d\mathrm{A}}\boldsymbol{\nabla}\mu_{\mathrm{A}}\right), \tag{1}$$

$$\boldsymbol{J}^d_{\mathrm{A}} = -\frac{1}{k_{\mathrm{B}}T}\left(\underline{L}_{\mathrm{A}d}\boldsymbol{\nabla}\mu_d + \underline{L}^d_{\mathrm{AA}}\boldsymbol{\nabla}\mu_{\mathrm{A}}\right), \tag{2}$$

where the phenomenological transport coefficients $\underline{L}_{dd}$, $\underline{L}_{d\mathrm{A}}$, $\underline{L}_{\mathrm{A}d}$, and $\underline{L}^d_{\mathrm{AA}}$ are symmetric second-rank tensors including the elastic contribution to diffusion [13, 17]. $\boldsymbol{\nabla}\mu_{\mathrm{A}}$ and $\boldsymbol{\nabla}\mu_d$ are chemical potentials of respectively atom A and point defect. By construction of the PD mechanism, we have the following constraint on fluxes:

$$\boldsymbol{J}_d = -s_d\boldsymbol{J}^d_{\mathrm{A}}, \tag{3}$$

where s_d is equal to

$$s_d = \begin{cases} +1, \text{ for } d = \mathrm{V}, \\ -1, \text{ for } d = \mathrm{I}. \end{cases} \tag{4}$$

Because the PD and atomic driving forces are independent, Eq. (3) yields $-s_d\,\underline{L}_{d\mathrm{A}} = \underline{L}_{dd}$ These relationships lead to PD diffusion driving forces depending on the atom chemical potential

$$\boldsymbol{J}_d = -\frac{1}{k_{\mathrm{B}}T}\,\underline{L}_{dd}\left(\boldsymbol{\nabla}\mu_d - s_d\boldsymbol{\nabla}\mu_{\mathrm{A}}\right). \tag{5}$$

2.1. Thermodynamics of diffusion including elasticity

The elimination of PDs at sinks necessarily entails the non-conservative nature of PDs. The creation or removal of PDs makes the number of lattice sites vary. For instance, an atom displaced from its original bulk lattice site to the surface or at a kink of the dislocation, creates both a vacancy at the original lattice site and an extra lattice site at the structural defect. If we assume no external stress at the surface or at the dislocation kink, putting the atom at the dislocation or at the stress-free surface is then equivalent. In presence of an internal stress generated by the dislocation, the elastic work associated with the exchange of atom between a stress-free reservoir and the solid at site x, is non zero. To account for this local stress at site x, we rely on a local equilibrium assumption. The elastic work is calculated as the one associated with the exchange of atom between the reservoir and an infinite

crystal under a uniform applied stress equal to the local stress at site x [18]. Since we treat the elastic work as a reversible work only depending on the final and initial states of the exchange path, we may deduce from it the PD formation enthalpy,

$$H_d^{\mathrm{F}}(x) = H_{d,0}^{\mathrm{F}} - \underline{\Omega}_{\mathrm{F}}^{d} : \underline{\sigma}(x). \tag{6}$$

In this equation, $H_{d,0}^{\mathrm{F}}$ is the PD enthalpy of formation in a stress-free crystal ($\underline{\sigma} = 0$). $\underline{\sigma}(x)$ is the local stress tensor at site x. The second term of the RHS corresponds to the work of inserting the PD (d) of volume $\underline{\Omega}_{\mathrm{F}}^{d}$ under the local stress $\underline{\sigma}(x)$. $\underline{\Omega}_{\mathrm{F}}^{d}$ is the formation volume of d which can be expressed as:

$$\underline{\Omega}_{\mathrm{F}}^{d} = \frac{1}{3} s_d \, \Omega_{\mathrm{at}} \, \underline{I} + \underline{\Omega}_{\mathrm{R}}^{d}, \tag{7}$$

where Ω_{at} is the atomic volume, $\underline{I}$ is the identity tensor, and $\underline{\Omega}_{\mathrm{R}}^{d}$ is the relaxation volume induced by d. Note that $\underline{\Omega}_{\mathrm{R}}^{d}$ is a second-rank tensor because the relaxation volume of a PD is not necessarily isotropic. Note that, in Appendix A, we provide an alternative approach to derive the same expression of PD formation enthalpy as Eq. (6) in an NVT-ensemble.

We treat PD as an infinitely dilute species (no interaction between PD). The corresponding PD chemical potential is then written as follows

$$\mu_d = k_{\mathrm{B}} T \ln\left(\frac{C_d}{C_d^{\mathrm{eq}}}\right), \tag{8}$$

where C_d is the atomic fraction of d in the system, and C_d^{eq} is the equilibrium atomic fraction of d. Such an approach yields PD chemical potentials locally depending on the internal strain/stress field generated by a dislocation. Note that, when PD is at local equilibrium, the corresponding local chemical potential is zero.

The equilibrium PD concentration, C_d^{eq}, is equal to the standard stress-free equilibrium concentration, $C_d^{\mathrm{eq},0}$, multiplied by a strain/stress field enthalpy contribution

$$C_d^{\mathrm{eq}} = C_d^{\mathrm{eq},0} \exp\left(-\frac{H_d^{\mathrm{el}}}{k_{\mathrm{B}} T}\right), \tag{9}$$

where H_d^{el} is the elastic contribution to the formation enthalpy of PD under the internal strain field $\underline{\epsilon}$.

$$H_d^{\mathrm{el}} = -s_d \, \Omega_{\mathrm{at}} \, \sigma_{\mathrm{v}} - \underline{\Omega}_{\mathrm{R}}^{d} : \underline{\sigma}, \tag{10}$$

where σ_{v} is the volumetric component of the local stress: $\sigma_{\mathrm{v}} = \mathrm{Tr}[\underline{\sigma}]/3$. By combining Eqs. (8)–(10), the PD chemical potential can be rewritten as:

$$\mu_d = \mu_d^0 + H_d^{\mathrm{el}}, \tag{11}$$

where $\mu_d^0 = k_{\mathrm{B}} T \ln\left(C_d / C_d^{\mathrm{eq},0}\right)$ is the PD chemical potential in a stress-free system.

We assume that the internal strain of the solid is solely generated by the dislocation. A strain tensor $\underline{\epsilon}$, having six independent components e_1 through e_6, can be written as

$$\underline{\epsilon} = e_{\mathrm{v}}\underline{I} + \begin{bmatrix} e_1 - e_{\mathrm{v}} & 0 & 0 \\ 0 & e_2 - e_{\mathrm{v}} & 0 \\ 0 & 0 & e_3 - e_{\mathrm{v}} \end{bmatrix} + \begin{bmatrix} 0 & \frac{1}{2}e_6 & \frac{1}{2}e_5 \\ \frac{1}{2}e_6 & 0 & \frac{1}{2}e_4 \\ \frac{1}{2}e_5 & \frac{1}{2}e_4 & 0 \end{bmatrix}, \tag{12}$$

where $e_{\mathrm{v}} = \frac{1}{3}\mathrm{Tr}[\underline{\epsilon}] = \frac{1}{3}(e_1 + e_2 + e_3)$.The volumetric strain is defined as $\underline{\epsilon}_{\mathrm{v}} = e_{\mathrm{v}}\underline{I}$; the tetragonal strain $\underline{\epsilon}_{\mathrm{t}}$ and the shear strain $\underline{\epsilon}_{\mathrm{s}}$ are the final two tensors in Eq. (12). By relying on the first-order linear approximation of the Hooke's law, we assume that the stress is proportional to the strain generated by the dislocation:

$$\underline{\sigma}_{ij} = \underline{C}_{ijkl}\underline{\epsilon}_{kl}, \tag{13}$$

where $\underline{C}$ is the elastic tensor. Eq. (10) can therefore be rewritten as:

$$\begin{aligned} H_d^{\mathrm{el}} &= -\frac{1}{3} s_d \Omega_{\mathrm{at}} \, \underline{C}_{iikl} \, \underline{\epsilon}_{kl} - \underline{\Omega}_{\mathrm{R},ij}^{d} \, \underline{C}_{ijkl} \, \underline{\epsilon}_{kl}, \\ &= -3\,K\,e_{\mathrm{v}} s_d \Omega_{\mathrm{at}} - \underline{P}^{\mathrm{sta},d} : \underline{\epsilon}, \\ &= -3\,K\,e_{\mathrm{v}}(\Omega_{\mathrm{R}}^{d} + s_d \Omega_{\mathrm{at}}) - \underline{P}^{\mathrm{sta},d} : (\underline{\epsilon}_{\mathrm{t}} + \underline{\epsilon}_{\mathrm{s}}), \end{aligned} \tag{14}$$

where $\underline{P}^{\mathrm{sta},d}$ is the elastic dipole tensor [2, 3] of PD (d) at the stable position with

$$\underline{P}_{kl}^{\mathrm{sta},d} = \underline{\Omega}_{\mathrm{R},ij}^{d} \, \underline{C}_{ijkl}, \tag{15}$$

$K = (\underline{C}_{11} + 2\underline{C}_{12})/3$ is the bulk modulus (Voigt notation), and

$$\Omega_{\mathrm{R}}^{d} = \mathrm{Tr}\left[\underline{\Omega}_{\mathrm{R}}^{d}\right] = \frac{\mathrm{Tr}\left[\underline{P}^{\mathrm{sta},d}\right]}{3\,K}. \tag{16}$$

Note that most modeling studies of sink biases solely account for the volumetric strain contribution, $\underline{\epsilon}_{\mathrm{v}}$, of the PD diffusion driving force [i.e., the first term of the RHS in Eq. (14)] because it is in general the main contribution to the PD formation energy [19]. In this case, the preferential creation site of a PD is determined by its formation volume $\Omega_{\mathrm{F}}^{d} = \Omega_{\mathrm{R}}^{d} + s_d\Omega_{\mathrm{at}}$ rather than its relaxation volume (cf. Tab. 1). In the investigated metals, the absolute value of the vacancy relaxation volume is smaller than the atomic volume. Therefore, the formation volumes of the vacancy and the SIA are both positive. Hence, they are preferentially created at sites of local tension ($e_{\mathrm{v}} > 0$) because more space is needed to insert the PDs into the system. Note that, in the present study, we also keep the non-volumetric contributions [i.e., the second term of the RHS in Eq. (14)], which are shown to be non-negligible in Refs. [20, 11] for the investigated metals.

Even though we assume that PDs are moving in a frozen dislocation microstructure, we must not ignore the atomic contribution to the diffusion driving force of a PD. As shown by Eq. (5), a chemical potential gradient of atoms generates a flux of PDs. Through the atom-PD exchanges and our definition of the local diffusion driving forces, we

include the elastic work of the moving atom exchanging its position with the PD in a non-homogeneous strain field. The elastic contribution to the formation enthalpy of an atom (A) of volume $\Omega_{\rm at}$ corresponds to the reversible elastic work to insert this atom into the system under the local stress $\underline{\sigma}$:

$$H_{\rm A}^{\rm el} = -\Omega_{\rm at}\,\sigma_{\rm v} = -3\,K\,\Omega_{\rm at}\,e_{\rm v}, \tag{17}$$

The chemical potential of this atom is given by

$$\mu_{\rm A} = \mu_{\rm A}^0 + H_{\rm A}^{\rm el} = \mu_{\rm A}^0 - 3\,K\,\Omega_{\rm at}\,e_{\rm v}, \tag{18}$$

where $\mu_{\rm A}^0$ is the chemical potential of A in an undeformed lattice. A non-zero strain gradient thus yields a non-zero gradient of the atom chemical potential

$$\boldsymbol{\nabla}\mu_{\rm A} = -3\,K\,\Omega_{\rm at}\boldsymbol{\nabla}e_{\rm v}. \tag{19}$$

Interestingly, sinks with a heterogeneous volumetric strain/stress field cannot be at steady state whenever PDs are at local equilibrium (with their gradient of chemical potential equal to zero). After Eq. (5) and (19), the atom chemical potential gradient would induce a net flux of PDs towards sinks. PD annihilation reactions at sinks would then either lead to the transformation or the motion of sinks. For instance, as long as there are dislocations, in thermal and irradiation conditions we expect net fluxes of PDs towards the dislocations together with the climbing motion of the dislocations. The higher the atomic volume and the internal strain gradient arising from the dislocation itself, the higher the PD flow and the resulting dislocation climbing rate. The climbing of the edge dislocation only stops if $\boldsymbol{\nabla}\mu_d = s_d\boldsymbol{\nabla}\mu_A$. This specific steady state may be reached when the interaction of PDs with the PDs sources and sinks including the dislocation itself is weak, or the PD diffusion coefficient is very small. These are situations where the equilibrium of PDs with respect to a free-stress surface or dislocation may not be established in the entire volume of the solid.

After Eqs. (5), (10) and (17), the elastic contribution to the total diffusion driving force of PD is thus equal to the gradient of the difference, $(H_d^{\rm el} - s_d H_{\rm A}^{\rm el})$, leading to

$$\boldsymbol{\nabla}H_{d{\rm A}}^{\rm el} = -3\,K\,\Omega_{\rm R}^d\boldsymbol{\nabla}e_{\rm v} - \underline{P}^{{\rm sta},d} : (\boldsymbol{\nabla}\underline{\epsilon}_{\rm t} + \boldsymbol{\nabla}\underline{\epsilon}_{\rm s}), \tag{20}$$

$$= -\underline{P}^{{\rm sta},d} : \boldsymbol{\nabla}\underline{\epsilon}. \tag{21}$$

There is a direct compensation between the atomic volume elastic terms of PD and atom A, which leads to a diffusion driving force depending on the PD relaxation volume only. Note that, though the final driving force is similar to the one introduced by the seminal works of Weertman[12] and Hirth and Lothe [4], our definition of the PD formation enthalpy disagrees. A PD chemical potential of a solid with no applied stress does include an atomic volume energy contribution proportional to the internal pressure. As mentioned before, we predict that both vacancies and interstitial atoms tend to form in tensile or less compressive regions. The preferential vacancy formation in the tensile region is counter-intuitive. However, if now the vacancy is already in the solid, during its diffusion it will exchange its position with a neighboring atom. Therefore, the Gibbs free energy change associated with exchanging the vacancy at site x_1 with local pressure $p_1 = -\sigma_{\rm v}(x_1)$ with a neighboring atom initially located at site x_2 with internal pressure $p_2 = -\sigma_{\rm v}(x_1)$ reads:

$$\Delta G = (p_2\Omega_{\rm F}^{\rm V} + p_1\Omega_{\rm at}) - (p_1\Omega_{\rm F}^{\rm V} + p_2\Omega_{\rm at}) = (p_2 - p_1)\Omega_R^{\rm V}. \tag{22}$$

Following the same reasoning, the change in Gibbs free energy corresponding to the diffusion of a SIA from site x_1 to site x_2 writes:

$$\Delta G = (p_2\Omega_{\rm F}^{\rm I} + p_2\Omega_{\rm at}) - (p_1\Omega_{\rm F}^{\rm I} + p_1\Omega_{\rm at}) = (p_2 - p_1)\Omega_R^{\rm I}. \tag{23}$$

The above two equations show that it is thermodynamically favored to have vacancies diffuse toward compressive regions and SIAs diffuse toward tensile regions, in agreement with previous literature works. Therefore, the equilibrium state of the system will indeed be with vacancies in compressive regions and SIAs in tensile regions, as it stems from the optimization of both atoms and point-defect energies: in other—admittedly qualitative—words, vacancies alone are preferentially created in the tensile regions but having vacancies in tensile regions necessarily means that atoms are in the compressive regions which is not energetically favorable, and therefore the system prefers to have vacancies in compressive regions and atoms in tensile regions to lower the global energy of the system.

From Eq. (11) and Eq. (19), we write the PD diffusion driving force as

$$\boldsymbol{\nabla}(\mu_d - \mu_{\rm A}) = k_{\rm B}T\,\frac{\boldsymbol{\nabla}C_d}{C_d} + \boldsymbol{\nabla}H_{d{\rm A}}^{\rm el}. \tag{24}$$

The second term of the RHS, the gradient of the elastic energy, corresponds to the so-called elastic drift force of the diffusion equation. This definition of the elastic drift force is in line with the previous elasto-diffusion studies (e.g., in Refs. [12, 4, 21, 22, 23, 10]).

2.2. Elasto-diffusion

Elastic interactions between PDs and extended defects modify the migration barriers of PDs. For a PD initially located at $\boldsymbol{r}$, jumping in a direction $\boldsymbol{h}$, we write the migration enthalpy as

$$H^{\rm mig}(\boldsymbol{r},\boldsymbol{h}) = H^{{\rm mig},\,0}(\boldsymbol{r},\boldsymbol{h}) + H_{\rm el}^{\rm sad}(\boldsymbol{r},\boldsymbol{h}) - H_{\rm el}^{\rm sta}(\boldsymbol{r}). \tag{25}$$

$H^{{\rm mig},\,0}(\boldsymbol{r},\boldsymbol{h})$ corresponds to the PD migration enthalpy in the system free of strain. $H_{\rm el}^{\rm sad}(\boldsymbol{r},\boldsymbol{h})$ and $H_{\rm el}^{\rm sta}(\boldsymbol{r})$ are the elastic contributions to the enthalpies at the saddle-point and stable configurations, respectively. They are deduced from the PD elastic dipoles at stable and saddle points, and their difference is equal to

$$H_{\rm el}^{\rm sad}(\boldsymbol{r},\boldsymbol{h}) - H_{\rm el}^{\rm sta}(\boldsymbol{r}) = -\left[\underline{P}^{\rm sad}(\boldsymbol{r},\boldsymbol{h}) - \underline{P}^{\rm sta}(\boldsymbol{r})\right] : \underline{\epsilon}(\boldsymbol{r}), \tag{26}$$

where $\underline{P}_{ij}^{\mathrm{sta}}$ and $\underline{P}_{ij}^{\mathrm{sad}}$ are the elastic dipoles of PD at the stable and saddle-point configurations, respectively.

The variation of the migration barriers with strain determines the change of the PD jump frequencies, thereby the variation of the transport coefficients. From the DFT migration barriers and elastic dipoles, we calculate the strain-dependent transport coefficient tensors $\underline{L}_{dd}$ using the KineCluE code [24]. Note that our calculated $\underline{L}_{dd}$ is in line with the expressions from Dederichs and Schroeder [13], and Trinkle [17], but the formalism from Dederichs and Schroeder is only valid for uncorrelated systems.

3. Sink bias calculation method

We consider two types of sinks: the straight edge dislocation and the edge dislocation loop. Their geometries and coordinate systems are shown in Fig. 1 and 2, respectively. The dislocation density (ρ) fixes the outer radius of the simulation domain (r_{out}): $r_{\mathrm{out}} = 1/\sqrt{\pi\rho}$ for a straight dislocation and $r_{\mathrm{out}} = \sqrt[3]{3/(4\pi\rho)}$ for a dislocation loop. The dislocation capture radius, r_{c}, delimits the area within which the elimination of PD is treated as an irreversible process. Ideally, the capture radius should be the one that produces a bias leading to the right climbing rate. An experimental investigation of the latter or atomic-scale simulations of the dislocation climbing, would facilitate the determination of the capture radius. Unfortunately, there is such data for pure iron only [25]. Here, we consider the capture radius as a variable of the model. Previous studies suggest that the dislocation capture radius, r_{c}, is of the order of the Burgers vector ($b_{\mathrm{v}} = ||\boldsymbol{b}_{\mathrm{v}}||$) [26, 27, 28, 29, 30, 31]. If the PD-dislocation core distance is within r_{c}, the lattice deformation is in general so high that PDs are absorbed by the dislocation by a diffusion-less mechanism in an extremely short period. However, PDs are emitted from the dislocation to maintain the PD concentration close to its equilibrium value near the dislocation core, at $r_{\mathrm{c}} \approx b_{\mathrm{v}}$. The standard approach is to set the PD concentration at the capture radius equal to its equilibrium value, whatever the value of the capture radius. As it will be shown in Section 5, such approach leads to sink biases which are strongly dependent on the capture radius.

PDs are steadily created by irradiation, then they diffuse and eliminate at sinks of the microstructure, leading to a stationary concentration of PDs at the outer radius and a net flux of PDs towards the investigated sink. We ignore the other reactions of PDs such as mutual recombination reactions between SIA and vacancy, or the agglomeration reactions of PDs. Diffusion of PDs in the vicinity of the investigated sink (beyond r_{c}) is described by the following diffusion equation:

$$\frac{\partial C_d}{\partial t} = -\boldsymbol{\nabla}\cdot\boldsymbol{J_d}. \tag{27}$$

The latter is solved in steady-state conditions (i.e., the time derivative of the PD concentration is set to zero: $\partial C_d/\partial t = 0$). We solve the equation $\boldsymbol{\nabla}\cdot(\underline{L}_{dd}\,\boldsymbol{\nabla}\mu_d) = 0$ by means of a finite-difference numerical scheme. We treat the dislocations as perfect sinks and assume that the concentration of PDs at the inner boundary surface, (Σ_{in}) of radius r_{c}, is equal to its local equilibrium value. PDs are massively produced under irradiation. Thus, we set the PD concentration at the outer boundary (Σ_{out}) to be much larger than its equilibrium value. Note that, in this case, the sink efficiencies and resulting bias parameters do not depend on the PD concentration at the outer boundary [32, 31].

The absorption efficiencies of d (Z_d) are evaluated by the current of d (I_d) entering the sink across the inner surface [32]:

$$Z_d = \frac{I_d}{D_d^0(C_d^{\mathrm{bulk}} - C_d^{\mathrm{in}})}, \tag{28}$$

where D_d^0 is the diffusion coefficient of d in the unstrained system, C_d^{bulk} and C_d^{in} are respectively the PD concentrations at the outer and inner boundaries, and

$$I_d = -\iint_{\Sigma_{\mathrm{in}}} \boldsymbol{J}_d\cdot\boldsymbol{n}\,\mathrm{d}\Sigma, \tag{29}$$

with $\boldsymbol{n}$ the vector normal to surface Σ_{in}. We define the bias factor as the relative difference between the sink absorption efficiencies

$$B = \frac{Z_{\mathrm{I}} - Z_{\mathrm{V}}}{Z_{\mathrm{I}}}. \tag{30}$$

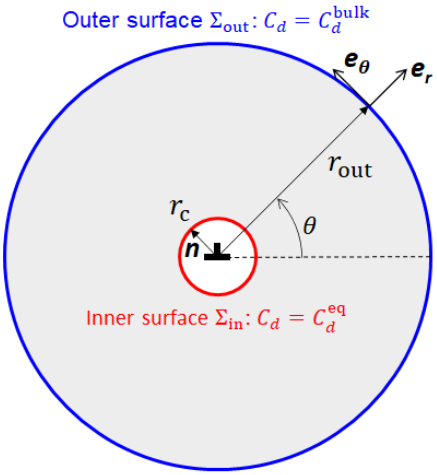

Figure 1: Geometry used to determine the point-defect absorption efficiency of a straight edge dislocation. At the outer boundary (Σ_{out}), the concentration is set to the bulk concentration C_d^{bulk}, whereas at the inner boundary (Σ_{in}) the concentration is set to the equilibrium one, C_d^{eq}.

3.1. Straight edge dislocation

Since a straight edge dislocation together with its boundary conditions has a translation symmetry along the

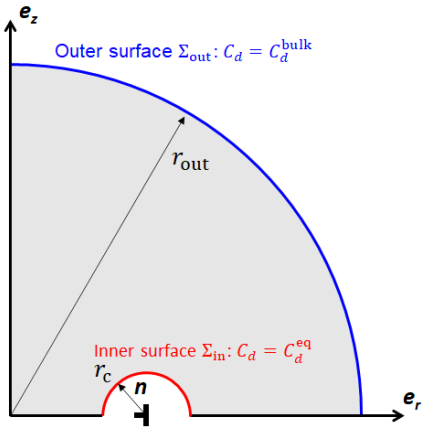

Figure 2: Geometry used to determine the point-defect absorption efficiency of an edge dislocation loop. At the outer boundary (Σ_{out}), the concentration is set to the bulk concentration C_d^{bulk}, whereas at the inner boundary (Σ_{in}) the concentration is set to the equilibrium one, C_d^{eq}. The point-defect fluxes across the surfaces delimited by the black boundary lines are equal to zero for symmetry reasons.

dislocation line, we ignore the diffusion of PDs and solute atoms along the dislocation line. We reduce the 3D calculation to a 2D calculation, by solving the problem of diffusion in the plane perpendicular to the dislocation. We introduce a polar coordinate system centered on the dislocation (cf. Fig. 1). Hence, the PDs diffusion zone is an annular region delimited by the capture radius of the dislocation (inner radius r_{c}), and the outer radius r_{out}. We rely on the planar strain approximation to compute the strain/stress field generated by a straight edge dislocation based on the analytical expressions given in Ref. [33, 34]. In this calculation, the anisotropic elasticity of the investigated metals has been systematically considered.

3.2. Edge dislocation loop

In the case of a dislocation loop, a full PD absorption study including elasto-diffusion requires to solve PD diffusion equations in three dimensions, which is computationally demanding. In the present work, to avoid the full 3D numerical integration, we neglect the elastodiffusion contribution to the PD absorption efficiency. The elastic strain of the dislocation loop enters the diffusion driving force only. This approximation allows us to model the dislocation loop as a torus of revolution. Since the torus geometry is invariant to rotation around its axis of revolution (the z-axis in Fig. 2), we reduce the 3D calculation to a 2D calculation. We solve the diffusion problem in the cross section plane of the torus (i.e., the z-r plane that contains the axis of revolution and is perpendicular to the circle of the torus, as shown in Fig. 2). Note that all such planes are equivalent because the effect of strain on PD jumps between planes is neglected. Furthermore, we rely on an isotropic approximation of the elastic field to compute the strain/stress field generated by an edge dislocation loop [35]. This allows us to calculate $H^{\text{el}}_{\text{tot},d}$ from available analytical formulae [31], namely:

$$H^{\text{el}}_{\text{tot},d} = -\frac{\text{sgn}(\Omega^d_{\text{R}})\, k_{\text{B}}\, T\, L_d}{\sqrt{(r+r_{\text{l}})^2+z^2}} \left[\frac{r_{\text{l}}^2 - r^2 - z^2}{(r_{\text{l}}-r)^2+z^2} \text{E}(k) + \text{K}(k) \right], \tag{31}$$

where $\text{sgn}(\Omega^d_{\text{R}})$ is the sign of the PD relaxation volume, r_{l} is the loop radius, E and K are respectively the elliptic integrals of the first and second kind,

$$k = \sqrt{\frac{4\, r\, r_{\text{l}}}{(r_{\text{l}}+r)^2+z^2}}, \tag{32}$$

and

$$L_d = \frac{1+\nu}{3\pi(1-\nu)}\, \mu\, b_{\text{v}}\, \frac{|\Omega^d_{\text{R}}|}{k_{\text{B}}T}, \tag{33}$$

with ν the Poisson's ratio and μ the shear modulus. Since only the volumetric strain is considered here, the results for a dislocation loop are independent of the loop orientation.

3.3. Orientation of the edge dislocation

In order to highlight the effect of the dislocation orientation on the point-defect absorption efficiency, we will compare simulation results for dislocations of different orientations.

First, we consider dislocations of energetically favorable orientations (**orientation 1**), which are characterized by:

- its normal vector to the glide plane: $\boldsymbol{n}_{\text{g}}^{(1)} = \frac{1}{\sqrt{2}}[1\,\bar{1}\,0]$ (Fe), $\frac{1}{\sqrt{3}}[1\,1\,1]$ (Ni, Al);
- its Burgers vector: $\boldsymbol{b}_{\text{v}}^{(1)} = \frac{a_0}{2}[1\,1\,1]$ (Fe), $\frac{a_0}{2}[1\,\bar{1}\,0]$ (Ni, Al);
- its unit line vector: $\boldsymbol{u}_{\text{l}}^{(1)} = \frac{1}{\sqrt{6}}[\bar{1}\,\bar{1}\,2]$ (Fe), $\frac{1}{\sqrt{6}}[1\,1\,\bar{2}]$ (Ni, Al).

Second, we consider the simplest edge dislocation, the $\langle 100\rangle\{010\}$-dislocation (**orientation 2**), even though it is less favorable energetically. This dislocation is characterized by:

- its normal vector to the glide plane: $\boldsymbol{n}_{\text{g}}^{(2)} = [1\,0\,0]$;
- its Burgers vector: $\boldsymbol{b}_{\text{v}}^{(2)} = a_0[0\,1\,0]$;
- its unit line vector: $\boldsymbol{u}_{\text{l}}^{(2)} = [0\,0\,1]$.

4. Simulation results

We apply the method presented in Section 2 and 3, to compute the PD absorption efficiencies and the elastic bias of dislocations in Fe, Ni, and Al. The physical parameters (e.g., the elastic dipoles, the elastic constants, etc.) of these metals are listed in Tab. 1. The elastic dipoles of PDs in Ni and Al are found in Refs. [11] and [10], respectively; those in Fe are calculated in the present study following the same DFT-based approach as presented in Ref. [40].

Table 1: Physical parameters of Fe, Ni and Al that are used in the simulations. $\boldsymbol{h}$ is the migration direction of PD. Ω is the atomic volume. The relaxation volume is obtained from the trace of the stable-point elastic dipole tensor.

Materials	bcc-Fe	Ni	Al
Lattice parameter [Å]	2.831 [36]	3.524 [37]	4.050 [10]
Burgers vector $b_{\mathrm{v}}^{(1)}$ (Orientation 1) [Å]	2.45	2.49	2.86
Burgers vector $b_{\mathrm{v}}^{(2)}$ (Orientation 2) [Å]	2.83	3.52	4.05
Capture radius $r_{\mathrm{c}}^{(1)}$ (Orientation 1) [nm]	0.98 ($\simeq 4b_{\mathrm{v}}^{(1)}$)	1.00 ($\simeq 4b_{\mathrm{v}}^{(1)}$)	1.43 ($\simeq 5b_{\mathrm{v}}^{(1)}$)
Capture radius $r_{\mathrm{c}}^{(2)}$ (Orientation 2) [nm]	1.70 ($\simeq 6b_{\mathrm{v}}^{(2)}$)	1.76 ($\simeq 5b_{\mathrm{v}}^{(2)}$)	1.62 ($\simeq 4b_{\mathrm{v}}^{(2)}$)
Elastic constants [GPa] ($\underline{C}_{11}$, $\underline{C}_{12}$, $\underline{C}_{44}$)	243, 145, 116 [38]	251, 150, 124 [39]	106, 60, 28 [10]
Formation enthalpy [eV] (vacancy, SIA)	2.18 [36], 4.08 [40]	1.65 [37], 4.07 [37]	0.76 [41], 2.00 [41]
Formation entropy [k_{B}] (vacancy, SIA)	4.10 [36], 0.05 [40]	1.82 [37], 12.7 [37]	2.40 [41], 16.0 [41]
Migration energy [eV] (vacancy, SIA)	0.70 [36], 0.34 [40]	1.09 [37], 0.14 [37]	0.605 [10], 0.105 [10]
Elastic dipole tensor [eV]			
Vacancy, stable point	$\begin{bmatrix} -2.839 & 0 & 0 \\ 0 & -2.839 & 0 \\ 0 & 0 & -2.839 \end{bmatrix}$	$\begin{bmatrix} -5.448 & 0 & 0 \\ 0 & -5.448 & 0 \\ 0 & 0 & -5.448 \end{bmatrix}$ [11]	$\begin{bmatrix} -3.238 & 0 & 0 \\ 0 & -3.238 & 0 \\ 0 & 0 & -3.238 \end{bmatrix}$ [10]
Vacancy, saddle point ($\boldsymbol{h}$ = [111] for Fe and [110] for Ni and Al)	$\begin{bmatrix} -2.217 & -1.641 & -1.641 \\ -1.641 & -2.217 & -1.641 \\ -1.641 & -1.641 & -2.217 \end{bmatrix}$	$\begin{bmatrix} -5.255 & -0.213 & 0 \\ -0.213 & -5.255 & 0 \\ 0 & 0 & 2.554 \end{bmatrix}$ [11]	$\begin{bmatrix} -2.866 & -0.080 & 0 \\ -0.080 & -2.866 & 0 \\ 0 & 0 & 1.000 \end{bmatrix}$ [10]
Dumbbell, stable point ([110] for Fe and [100] for Ni and Al)	$\begin{bmatrix} 23.752 & 4.728 & 0 \\ 4.728 & 23.752 & 0 \\ 0 & 0 & 27.906 \end{bmatrix}$	$\begin{bmatrix} 25 & 0 & 0 \\ 0 & 24.792 & 0 \\ 0 & 0 & 24.792 \end{bmatrix}$ [11]	$\begin{bmatrix} 19.652 & 0 & 0 \\ 0 & 18.518 & 0 \\ 0 & 0 & 18.518 \end{bmatrix}$ [10]
Dumbbell, saddle point ($\boldsymbol{h}$ = [111] from [110] to [101] for Fe; and $\boldsymbol{h}$ = [110] from [100] to [010] for Ni and Al)	$\begin{bmatrix} 23.838 & 2.845 & -0.696 \\ 2.845 & 22.529 & 2.845 \\ -0.696 & 2.845 & 23.838 \end{bmatrix}$	$\begin{bmatrix} 25.438 & 1.492 & 0 \\ 1.492 & 25.678 & 0 \\ 0 & 0 & 25.411 \end{bmatrix}$ [11]	$\begin{bmatrix} 19.498 & 1.133 & 0 \\ 1.133 & 19.498 & 0 \\ 0 & 0 & 19.034 \end{bmatrix}$ [10]
Formation volumes ($\Omega_{\mathrm{F}}^{\mathrm{V}}$, $\Omega_{\mathrm{F}}^{\mathrm{I}}$)	$+0.75\,\Omega$, $+1.17\,\Omega$	$+0.57\,\Omega$, $+0.98\,\Omega$	$+0.60\,\Omega$, $+1.50\,\Omega$
Relaxation volumes ($\Omega_{\mathrm{R}}^{\mathrm{V}}$, $\Omega_{\mathrm{R}}^{\mathrm{I}}$)	$-0.25\,\Omega$, $+2.17\,\Omega$	$-0.43\,\Omega$, $+1.98\,\Omega$	$-0.40\,\Omega$, $+2.50\,\Omega$

To begin with, we investigate the impact of a change of dislocation microstructure (dislocation density) on the dislocation bias for two orientations of the straight edge dislocation and edge dislocation loop. Then we show the effect of temperature on dislocation bias, and finally we discuss the effect of the dislocation orientation and the PD redistribution around the straight dislocation and dislocation loop.

The capture radius r_c of a dislocation is, by convention, an integer multiple of b_{v}. In the following studies, r_c of the straight dislocation or the dislocation loop is set to the values listed in Tab. 1 so that all strains generated by the straight dislocation or dislocation loop are within $\pm 3\,\%$, in order to be within the usual range of application of linear elasticity theory [23, 2, 3].

The validation of the numerical approach is given in Appendix B.

4.1. Effect of dislocation density

In this section, the simulation temperature is set to 600 K, which is close to the working temperature of nuclear reactors. In Fig. 3, we present the results of the elastic bias (B) and the absorption efficiencies of vacancies (Z_{V}) and SIAs (Z_{I}) as functions of the straight dislocation density $\rho = 1/(\pi r_{\mathrm{out}}^2)$. These calculations were performed for two orientations and include the full elastic effects on both the elastodiffusion transport coefficient and the driving force, i.e., the elastic drift. Case 1 considers dislocations with Orientation 1, while Case 2 includes dislocations with Orientation 2. In Fig. 4, similar results are shown for the dislocation loop, again for two different orientations of the dislocation loop. Note that in this case elastic effects are only included in the elastic drift part and not in the transport coefficient, due to computational limitations. In all of these cases, both the PD absorption efficiency and the elastic bias show a monotonic increase as a function of dislocation density.

4.2. Effect of temperature

The bias factor also depends on temperature. In Fig. 5, we plot the dislocation bias obtained at different temperatures for a straight dislocation and a dislocation loop. The lower the temperature, the higher is the dislocation bias. To explain this tendency, we consider the PD absorption efficiency, Z_d. By combining Eqs. (1), (24), (28), and (29),

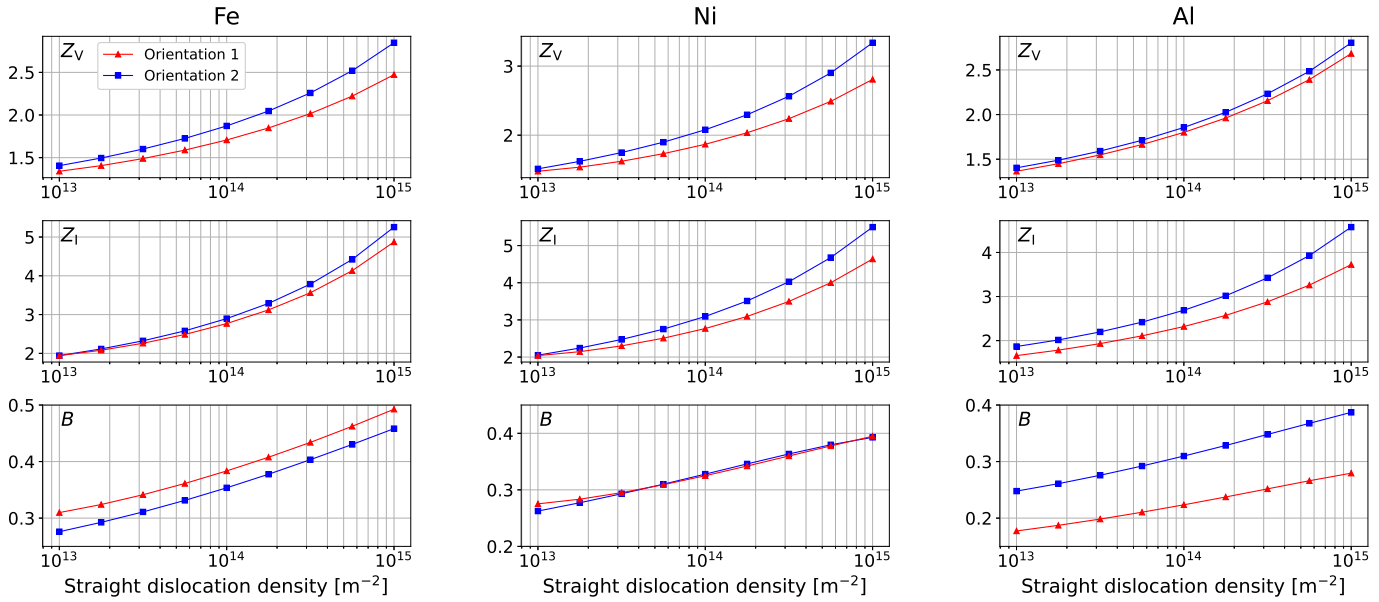

Figure 3: PD absorption efficiency and elastic bias of straight edge dislocations of two different orientations in Fe, Ni, and Al. The simulation temperature is set to 600 K.

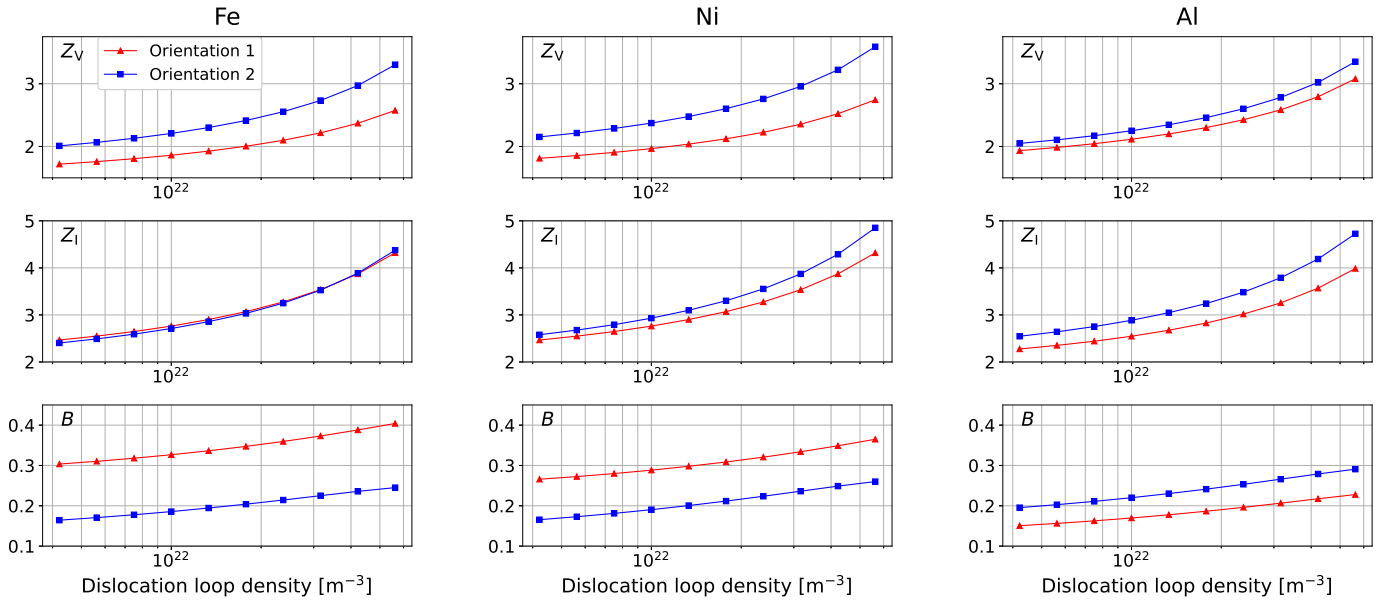

Figure 4: PD absorption efficiency and elastic bias of edge dislocation loops of two different orientations in Fe, Ni, and Al. The simulation temperature is set to 600 K.

we have

$$Z_d = -\iint_{\Sigma_{\text{in}}} \frac{\underline{D}_d C_d}{D_d^0 (C_d^{\text{bulk}} - C_d^{\text{in}})} \left(\frac{\boldsymbol{\nabla} C_d}{C_d} - \frac{\boldsymbol{\nabla} H_{\text{tot},d}^{\text{el}}}{k_{\text{B}} T} \right) \cdot \boldsymbol{n} \, \mathrm{d}\Sigma, \tag{34}$$

where $\underline{D}_d = \underline{L}_{dd}/C_d$. The dislocation bias is non-zero only when the second term in the parenthesis of Eq. (34), i.e., $\boldsymbol{\nabla} H_{\text{tot},d}^{\text{el}}/(k_{\text{B}}T)$, is non negligible with respect to the concentration gradient contribution (first term). This second term decreases with temperature by a factor $k_{\text{B}}T$. We check that the prefactor before the parenthesis in Eq. (34) is nearly temperature-independent. Therefore, we may conclude that Z_d decreases with temperature, towards the elasticity-free value (dashed lines in Fig. 5).

4.3. Effect of the orientation of the dislocation

By comparing the results obtained for both orientations in Fig. 3, we highlight the effect of the dislocation orientation on the PD absorption efficiency. We observe that Z_V and Z_I obtained for the dislocations with orientation

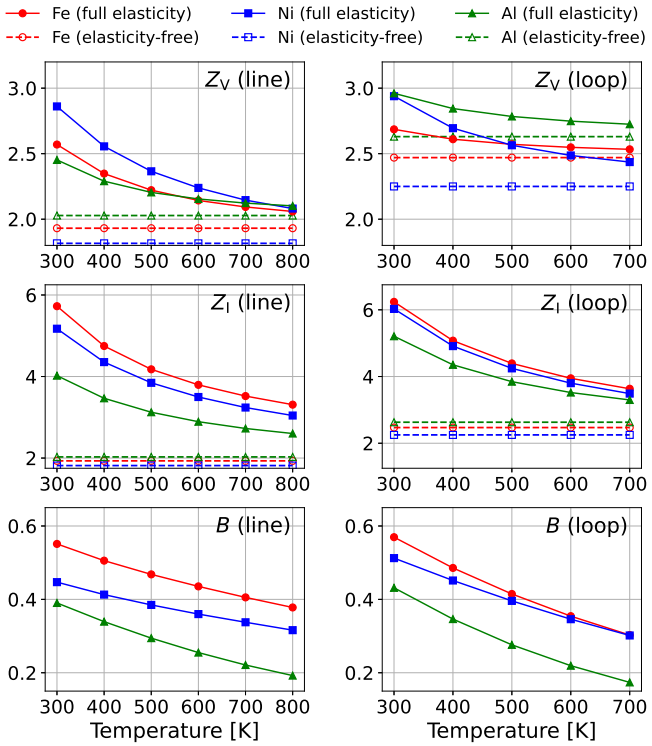

Figure 5: PD absorption efficiency and elastic bias of a straight edge dislocation (left) and a dislocation loop (right) as functions of temperature. The dislocation density is set to $3 \times 10^{14}\,\mathrm{m}^{-2}$ for the straight dislocation and to $4 \times 10^{22}\,\mathrm{m}^{-3}$ for the dislocation loop. The loop radius is set to 10 nm.

2 are higher than those obtained for the dislocations with orientation 1, leading to a significant change of the elastic bias in Fe and Al. The ratio between the bias factors of Cases 1 and 2 is about 1.1 in Fe and about 0.5 in Al, whereas it is almost 1 in Ni.

In Fig. 4, we show the elastic bias for an edge dislocation loop. As for the straight edge dislocation, a significant modification of the elastic bias is observed when the dislocation orientation is changed. Here again, Z_V and Z_I obtained for the dislocations with orientation 2 are higher than those obtained for the dislocations with orientation 1. The ratio between the bias factors of Cases 1 and 2 is about 1.2 in Fe, 1.5 in Ni, and 0.7 in Al.

The difference of elastic bias and point-defect distribution near dislocations of the two investigated orientations results from the differences of the elastic fields induced by these dislocations. The strength of the elastic field is proportional to the Burgers vector (b_v). Since the Burgers vector of the dislocation with orientation 1 ($b_\mathrm{v}^{(1)}$) is smaller than that with orientation 2 ($b_\mathrm{v}^{(2)}$), the magnitude of the elastic field generated from the latter is larger than that generated by the former. Therefore, the dislocation/PD interaction is stronger for orientation 2. This explains why dislocations with orientation 2 have higher PD absorption efficiencies (Z_V, Z_I) than those with orientation 1. However, since the magnitude of this effect is different for the vacancy and the SIA, the resulting bias is not always higher for the dislocations with orientation 2. Hence, we expect the climbing rate of the less stable dislocation line and loop to be higher in Al and smaller in Fe.

In Figs. 6 and 7, we plot the composition maps of vacancies and SIAs around the straight and loop dislocations for each of the two orientations. In the case of orientation 1, the PD-depleted regions are smaller than those of orientation 2, especially in Ni and Al. Besides, the shapes of the PD-depleted regions resulting from the PD fluxes depend as well on the orientation of the dislocation. In alloys, the PD fluxes towards sinks induce fluxes of atoms that produce changes of the alloy composition close to sinks (the so-called radiation-induced segregation). Therefore, we expect an effect of the dislocation orientation on radiation-induced segregation. If the effect of orientation on the PD-depleted regions seems to be more spectacular for the straight dislocation than for dislocation loop, it is simply because the elasto-diffusion contribution was neglected in the present dislocation loop study. We will see below that the strain effect on PD diffusion and subsequent PD distribution at sinks highly depends on the dislocation orientation.

The orientation-dependent elastic field produces different elastodiffusion behaviors in the vicinity of the straight edge dislocation. We plot in Figs. 8–10 the deviation between the PD elastodiffusion coefficients and the elasticity-free coefficients ($\Delta D_{d,ij} = D_{d,ij} - D^0_{d,ij}$) around the edge dislocations, with the two investigated orientations, respectively in Fe, Ni, and Al. Note that for the strain-free coefficients, we have $D^0_{d,11} = D^0_{d,22} = D^0_d$ because the non-deformed crystal is isotropic for PD diffusion. Besides, due to cubic symmetry, $D^0_{d,12} = 0$. A positive $\Delta D_{d,ij}$ entails an increase of $D_{d,ij}$ when the effect of the local deformation is accounted for. According to our calculations, the regions of positive $\Delta D_{d,ij}$ are strongly related to the dislocation orientation, especially $\Delta D_{d,11}$ and $\Delta D_{d,22}$.

We also notice a different elastodiffusion behavior in the three investigated metals. Since we observe a higher absolute value of $\Delta D_{\mathrm{I},ij}/D^0_\mathrm{I}$ in Fe, we may conclude that the local deformation-induced change of SIA diffusion coefficient in Fe is more significant than those in Ni and Al. As for the vacancy diffusion, the effect of strain on $D_{\mathrm{V},ij}$ is more significant in Ni than in the two other metals. Overall, the absolute value of $\Delta D_{d,ij}/D^0_d$ is the smallest in Al, showing that the effect of strain on PD diffusion is relatively weak in Al.

5. What choice of capture radius?

In the previous section, we have highlighted an effect of the microstructure (dislocation density), the temperature, and the orientation of the dislocation, on the bias factor. In this section, we analyse the sensitivity of the absorption efficiencies and the resulting bias factor to the capture radius and PD concentrations at this capture radius.

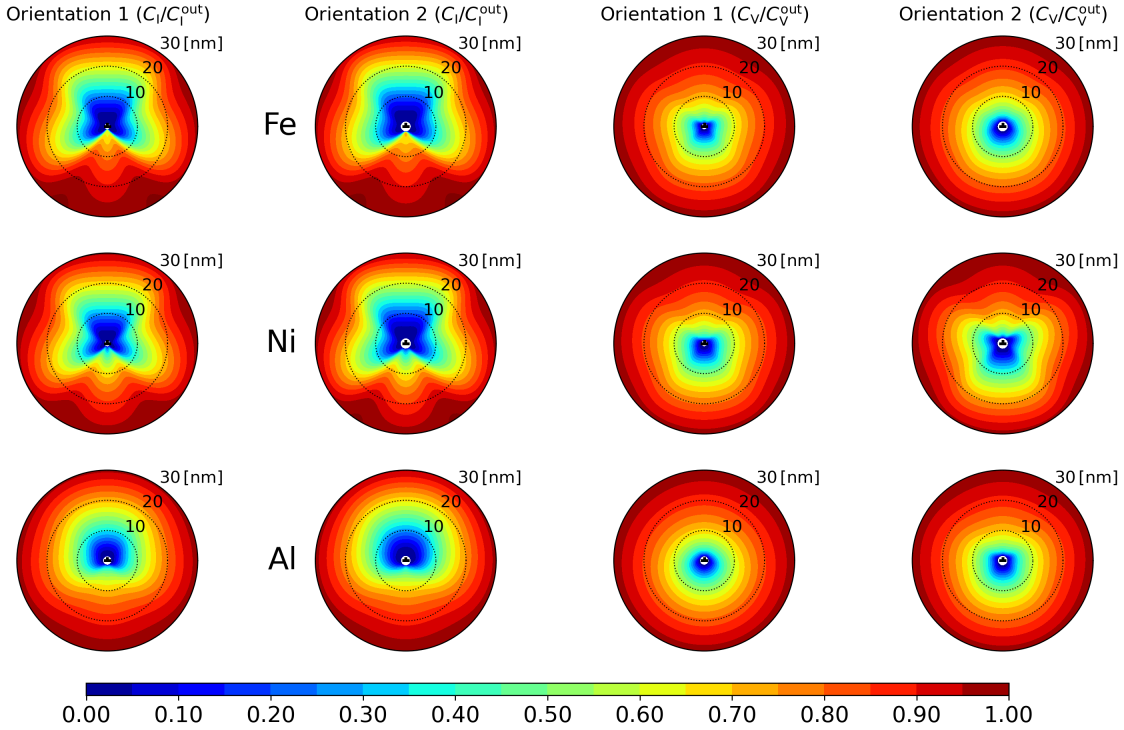

Figure 6: SIA and vacancy concentration maps around obtained from straight edge dislocations of two different orientations. The point-defect concentration (C_d) is normalized by the one at the outer boundary (C_d^{out}). The dislocation density is set to $3 \times 10^{14}\,\text{m}^{-2}$ (corresponding to $r_{\text{out}} = 32\,\text{nm}$) and the temperature is set to 600 K.

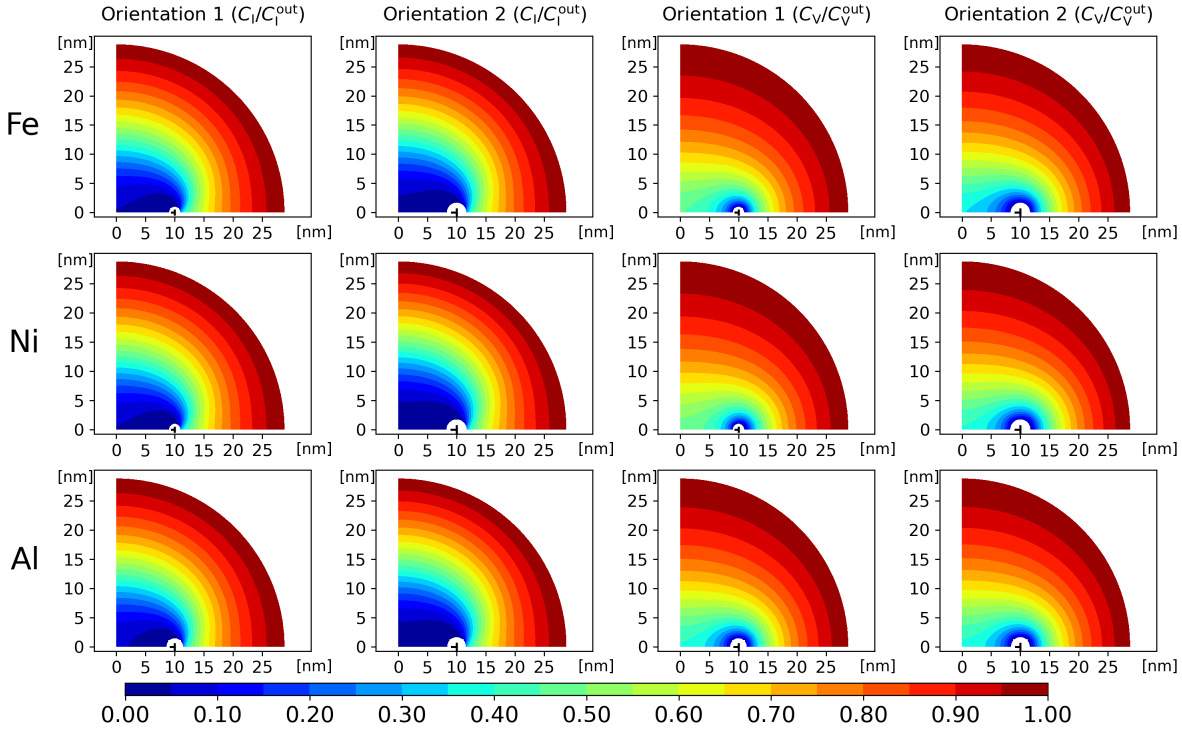

Figure 7: SIA and vacancy concentration maps around obtained from edge dislocation loops of two different orientations. The point-defect concentration (C_d) is normalized by the one at the outer boundary (C_d^{out}). The dislocation loop density is set to $10^{22}\,\text{m}^{-3}$ (corresponding to $r_{\text{out}} = 29\,\text{nm}$) and the temperature is set to 600 K.

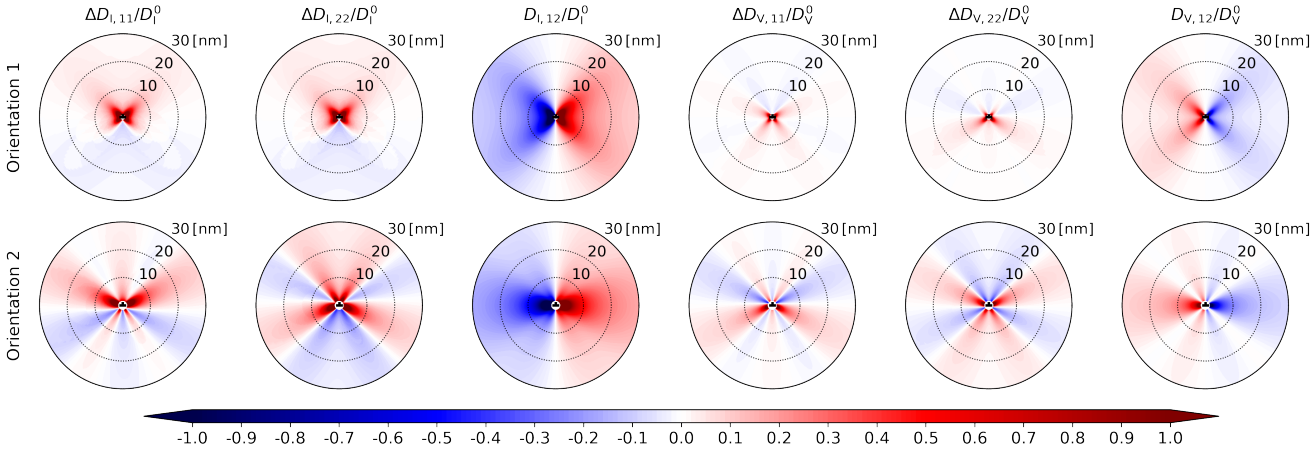

Figure 8: Deviation between the PD diffusion coefficient ($D_{d,ij}$) and the elasticity-free coefficient (D_d^0) around edge dislocations of two different orientations in Fe. The dislocation density is set to $3 \times 10^{14}\,\mathrm{m}^{-2}$ (corresponding to $r_{\mathrm{out}} = 32\,\mathrm{nm}$). The temperature is set to 600 K. The tensor $D_{d,ij}$ is expressed in polar coordinates.

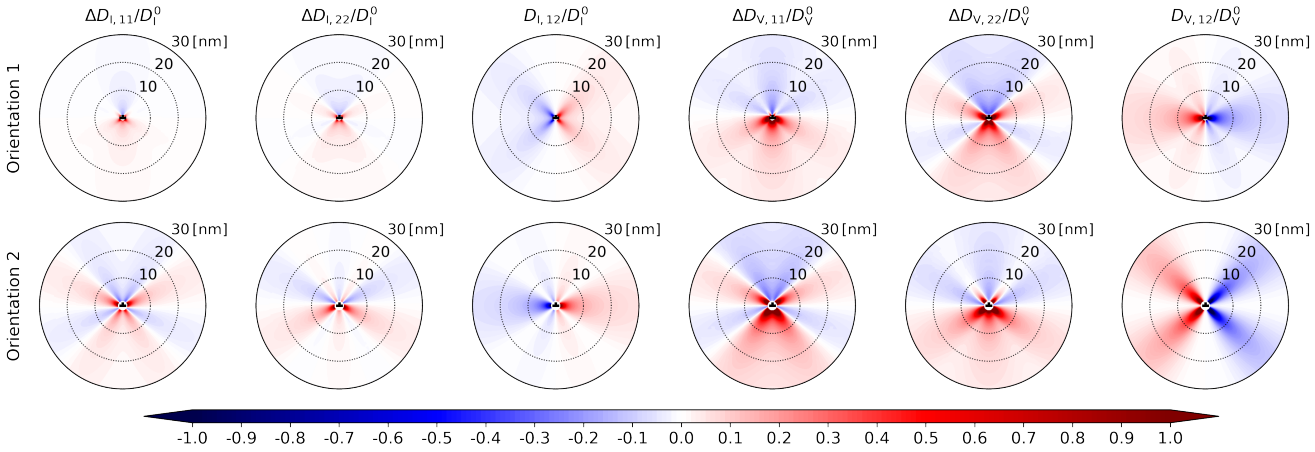

Figure 9: Deviation between the PD diffusion coefficient ($D_{d,ij}$) and the elasticity-free coefficient (D_d^0) around edge dislocations of two different orientations in Ni. The dislocation density is set to $3 \times 10^{14}\,\mathrm{m}^{-2}$ (corresponding to $r_{\mathrm{out}} = 32\,\mathrm{nm}$). The temperature is set to 600 K. The tensor $D_{d,ij}$ is expressed in polar coordinates.

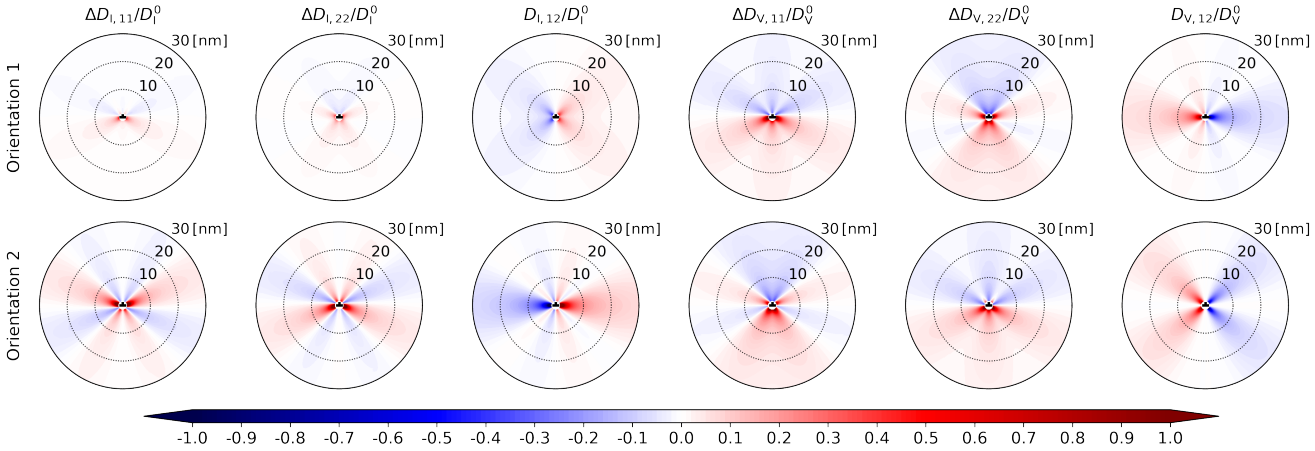

Figure 10: Deviation between the PD diffusion coefficient ($D_{d,ij}$) and the elasticity-free coefficient (D_d^0) around edge dislocations of two different orientations in Al. The dislocation density is set to $3 \times 10^{14}\,\mathrm{m}^{-2}$ (corresponding to $r_{\mathrm{out}} = 32\,\mathrm{nm}$). The temperature is set to 600 K. The tensor $D_{d,ij}$ is expressed in polar coordinates.

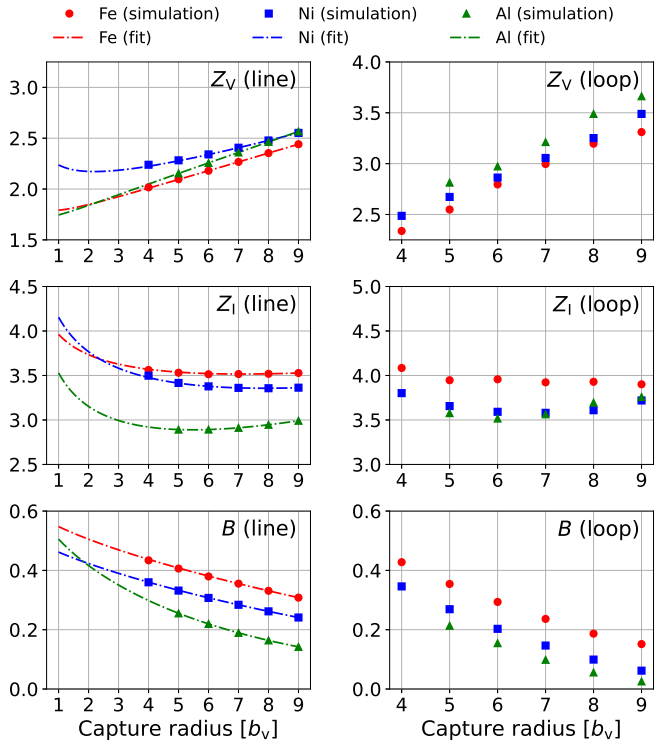

Figure 11: PD absorption efficiency and elastic bias of a straight edge dislocation (left) and a dislocation loop (right) in function of the capture radius. The simulation temperature is set to 600 K and the dislocation density to $3 \times 10^{14}\,\mathrm{m}^{-2}$ for the straight dislocation and $4 \times 10^{22}\,\mathrm{m}^{-3}$ for the dislocation loop. The loop radius is set to 10 nm.

The model of PD absorption efficiency in a strain-free medium, provides an explicit analytical expression of the efficiency with respect to the capture radius [32]

$$Z_\mathrm{d} = \frac{\eta}{\ln(r_\mathrm{out}/r_\mathrm{c}^\mathrm{d})}, \tag{35}$$

where η is a geometric parameter. For an isolated dislocation, its theoretical value is 2π. Z_d increases with the capture radius, and does not depend on the temperature or the material. As explained in the previous section, the impact of elastic interactions decreases with temperature. Therefore, at high temperature, we may expect the elastic effect to be negligible. In this case, the increase of Z_d with the capture radius, r_c^d, can be predicted by Eq. (35).

We study here the most stable dislocations (orientation 1), and we calculate the variation of the dislocation absorption efficiency and bias factor with the capture radius and the PD concentrations at the capture radius. The results are plotted in Fig. 11, both for the straight dislocation and the dislocation loop. Before going further into the analysis of the simulation results, we would like to emphasize the very high magnitude of the predicted strain field close to the dislocation core, which can go up to 10%. Such a high strain cannot be treated with linear elasticity theory and the elastic dipole formulation [e.g., Eqs. (10) and (26)], which is usually considered valid up to a few percents only. According to our simulation results, differently from the strain-free model predictions, the dislocation absorption efficiency of the self-interstitial, Z_I, of both the straight and loop dislocation does not increase with the capture radius, whereas Z_V does. Since the elastic strain and its impact on the PD diffusion is higher close to the dislocation core, the smaller the capture radius, the higher the elastic contribution to the PD absorption efficiency. However, the interaction of the strain field with SIAs is greater than that with vacancies because the lattice distortion induced by a SIA is stronger than the one induced by a vacancy. Therefore, the variation of Z_I with r_c is different from that of Z_V. A parabolic fit of the variation of Z_I with r_c highlights the non-monotonous variation of Z_I for Al, which cannot be predicted from the analytical law [Eq. (35)]. The resulting dislocation bias systematically decreases with the capture radius, for both the straight dislocation and the dislocation loop. For instance, for a straight dislocation line, the variation of the capture radius from $9\,b_\mathrm{v}$ to $5\,b_\mathrm{v}$ increases the dislocation bias by a factor of about 1.5 in Fe, Ni and Al. This increase is too high to be ignored.

Note that there is no general consensus on the method to be used to set the value of the capture radius, r_c. The criteria that are widely used in the literature, are either related to the limitations in the strain/stress field of the linear elasticity theory [23], or to the limitations of a first order Onsager formulation of the PD flows [42, 43, 28, 44, 31, 45]. Within the former condition, the capture radius has to be large enough so that the linear elastic theory applies. Within the latter condition, the diffusion driving forces should be small enough so that the PD elastic drift force can still be introduced as a first order correction term of the diffusion driving force [42, 43]. Within our formulation, the elastic drift force corresponds to the second term of the RHS of Eq. (1), r_c is fixed such that the variation of H_d^el is of the same order of magnitude as the thermal energy fluctuations

$$\left\|\boldsymbol{\nabla} H_d^\mathrm{el}\right\|_{r=r_\mathrm{e}} \simeq \frac{k_\mathrm{B}T}{b_\mathrm{v}}, \tag{36}$$

where the Burger vector, b_v, is introduced as the characteristic length of the strain heterogeneity generated by the dislocation. According to these criteria, one obtains a bottom value of the capture radius. We choose to call the latter, the energy cutoff radius, r_e^d, because it determines the domain of validity of the diffusion equations, but does not really provide a physical justification for the choice of the PD capture radius. After Eq. (20), r_e should depend on the elastic properties of the material, the nature of the PDs, and temperature. For instance, for a straight dislocation, under the assumption of isotropic elasticity and neglecting the non-volumetric strains, the capture radius of PD d is obtained from Eqs. (20) and (36) and written as

$$r_\mathrm{e}^d \simeq \sqrt{\frac{\mu}{3\pi}\,\frac{1+\nu}{1-\nu}\,\frac{|\Omega_\mathrm{R}^d|}{k_\mathrm{B}T}}\,b_\mathrm{v}, \tag{37}$$

where μ is the shear modulus and ν is the Poisson's ratio of the material. In Fe, Ni, and Al, we obtain that $r_e^I \simeq 5\,b_v$ and $r_e^V \simeq 3\,b_v$ at 600 K.

Another approach consists in relating the PD capture radius of the dislocation to its climbing rate. For a straight dislocation, the rate theory predicts that the climbing rate is related to the difference between the absorption efficiencies of SIAs and vacancies (Z_d with $d = V, I$) defined by Eq. (28) [46, 47, 48, 49]:

$$v_{cl} = \frac{Z_V}{b_v} D_V^0 (C_V^{bulk} - C_V^{in}) - \frac{Z_I}{b_v} D_I^0 (C_I^{bulk} - C_I^{in}). \quad (38)$$

Under irradiation, both vacancies and self-interstitials are generated. Hence, both their contribution to the dislocation climbing rate have to be accounted for. Since the capture radii of these PDs are not necessarily equal, Eq. (38) does not determine the pair of capture radii in a univocal way. However, in thermal conditions, we may neglect the self-interstitial contribution to the dislocation climbing because the self-interstitial formation energy in metals is generally much larger than the vacancy formation energy. When the climbing of a dislocation results from a supersaturation of vacancies only, the second term of the RHS of Eq. (38) is zero. Provided the variation of Z_V with the capture radius is known, we rely on Eq. (38), to deduce the vacancy capture radius. We may rely on our calculations of Z_V presented in Fig. 11, to deduce the capture radius in Fe, Al and Ni. The climbing rate can be measured by transmission electron microscopy or deduced from atomic scale simulations. Note that the surrounding microstructure and temperature have to be carefully determined because they govern the bulk concentration of point defects. Such a multiscale investigation of the capture radius has been performed in Fe [50, 25]. The molecular dynamics simulations of the dislocation climbing resulting from vacancy elimination were performed at high temperature [50]. The elastic interactions were not expected to be prominent at high temperature and the corresponding absorption efficiency was deduced from Eq. (35). Yet, due to the interactions between the dislocations of the simulated dislocation dipole and their periodic images, the constant η was treated as a fitting parameter [25]. The best quantitative agreement with atomistic simulations of Ref. [50] has been obtained for $\eta = 12.8 \sim 4\pi$ and $r_c^V \sim 4\,b_v$ in bcc Fe at $T > 800$ K. This value happens to be close to the elastic cutoff radius deduced from a condition of validity of the diffusion equation based on the linear elasticity theory. However, we show in Fig. 11 that at the investigated temperature (600 K) the variation of Z_V with the capture radius differs from the high-temperature/elasticity-free one. Therefore we expect a low-temperature capture radius which is not necessarily consistent with the energy cutoff radius. Besides, the elastic interactions between SIAs and dislocations are in general greater than those between vacancies and dislocations. In all these cases, the absorption efficiencies cannot be expressed in the form of Eq. (35). As for the dislocation loop, very few studies provide a calculation of the absorption efficiencies with respect to the capture radius. One usually assumes that Z_d is close to the one of a straight edge dislocation. This hypothesis is not valid when the loop radius is not large enough with respect to the capture radius, as shown in Fig. 11. Our calculations provide a full database of the variation of Z_d with respect to the capture radius, as long as the latter is above the energy cutoff radius. The Molecular Dynamics method is the appropriate method to investigate off-lattice diffusion processes, provided that diffusion is fast enough to be simulated by a Molecular Dynamics methods with time steps of a few femtoseconds.

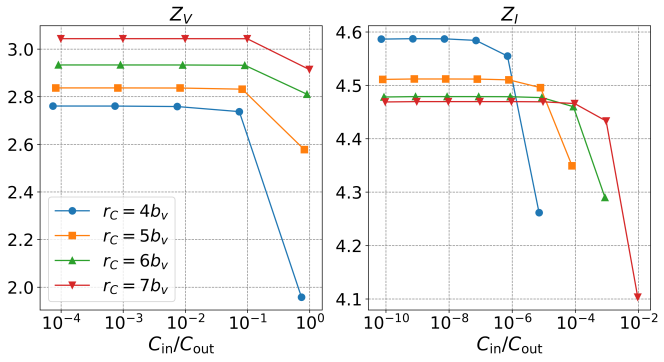

Figure 12: Vacancy (left) and SIA (right) absorption efficiency of a straight edge dislocation in Ni as a function of the capture radius and the ratio between the concentrations at the inner (C_{in}) and the outer boundaries (C_{out}). The simulation temperature is set to 600 K.

Unless the annihilation/creation reaction at the dislocation core is the limiting reaction, diffusion near the sink should not determine the PD absorption efficiency. Therefore, the PD absorption efficiency should mainly depend on PD long-range diffusion far from the dislocation, and should not depend on the choice of the capture radius and the value of the PD concentration at the capture radius, $C_{in} = C_d(r_c)$. We should therefore be able to obtain a robust estimate of the absorption efficiency from a calculation of the long-range diffusion in the diffusion zone bounded by r_c and r_{out}.

We observe in Figs. 11 and 12 that, although PD absorption efficiencies strongly vary with the capture radius, there is a range in PD concentration, $C_{in} = C_d(r_c)$, for which PD absorption efficiencies are constant. We explain it from the strongly non-linear increase of the PD concentrations between the capture radius and the outer radius, as shown in Figs. 6 and 7. This increase is driven by the overall reduction of the steady state gradient of chemical potential between r_c and r_{out}. Hence, whatever the value of C_{in} at the capture radius, the sharp increase of C_d insures a constant concentration gradient at a given capture radius. Therefore, as a preliminary approach, we may extract from the low-C_{in} values of Z_I and Z_V with the capture radius, the asymptotic variation of Z_I and Z_V at low capture radius down to the smallest possible distance between a PD and the dislocation, which is $r_c = b_v$.

We use results obtained from $r_c = 7$–$9\,b_v$ as input data of the fitting (i.e. the training set), and the ones obtained from $r_c = 4$–$6\,b_v$ (5–$6\,b_v$ in Al) as input data to check the fitting (i.e. the validation set). We have checked that the variation of Z_V for a strain edge dislocation follows the global tendency as described by Eq. (35), while Z_I does not follow this tendency. In order to choose a hypothesis function able to describe both Z_V and Z_I for a straight dislocation, this function has a similar form to the expression of Eq. (35) but with two additional correction terms:

$$h(r_c) = \theta_0 + \frac{\theta_1}{\ln(r_{out}/r_c)} + \theta_2 \ln(r_{out}/r_c), \qquad (39)$$

with θ_0, θ_1, and θ_2 the fitting parameters. We plot in Fig. 11 the obtained fitting functions of Z_V, Z_I, and the elastic bias. The above functions not only reproduce well the training data set ($r_c = 7$–$9\,b_v$), but their extrapolation is in very good agreement with the validation data set ($r_c = 4$–$6\,b_v$ in Fe, Ni and $r_c = 5$–$6\,b_v$ in Al), with an error smaller than 1%. The elastic bias of an edge dislocation thus corresponds to the extrapolated value of the fitted function, at $r_c = b_v$. The resulting bias is found to be larger than the standard ones calculated at a larger capture radius. The same approach could be applied to the computation of the elastic bias of a dislocation loop. However, the hypothesis function for the dislocation loop bias is more complex than that for the dislocation line because it also depends on the ratio between the capture radius and the loop radius, as well as on the ratio between the loop radius and the outer radius. To fit such a complex function (with at least two more parameters to be fitted), more input data would be required. Such study hence requires further investigations.

6. Conclusions

In this work, we calculate the vacancy and self-interstitial absorption efficiency and the resulting bias factor of a straight dislocation and dislocation loop in Fe, Ni and Al metals, by numerically solving the point-defect diffusion equations including the elastodiffusion contribution. The effect of strain on the atomic volume contribution to the PD formation volume—which results from the non-conservative nature of PDs—is accounted for, leading to a new separation of the PD diffusion driving force between the PD and atom chemical potentials. Let us emphasize again that the main point of this derivation is to show that in a strain field, the point defect formation energy and point defect diffusion are controlled by two different driving forces, which is rather unusual as the diffusion driving force is generally a thermodynamic driving force. Here the difference comes from the diffusion mechanism, i.e., point defect diffusion necessarily induces atomic diffusion and the thermodynamic driving forces for atoms and point defects are different. We highlight the strong variation of the dislocation absorption efficiency together with the resulting bias factor with the dislocation density, the temperature, the orientation of the dislocation line, and the capture radius. We summarize below the most relevant results obtained from our simulation.

- Counter-intuitively, when the atomic volume contribution to the vacancy formation is accounted for, vacancies are more likely to form in the compressive regions, even though they tend to diffuse toward the tensile region of the dislocation.
- The elastodiffusion behavior is sensitive to the dislocation orientation. The difference in dislocation orientation leads to a spectacular modification of the anisotropic PD trajectories. This should lead to variations of the radiation induced segregation with the dislocation orientation in alloys [51]. The investigation of the solute redistribution in the vicinity of sinks could provide a confirmation of the present result.
- To be valid, the linear elasticity approximation requires the capture radius to be above a certain value. An artificial spatial division of the simulation region using such a cut-off radius results in a strongly capture radius-dependent absorption efficiency and dislocation bias. The choice of its value should be chosen in such a way that the absorption efficiency of point defects leads to the measured climbing rate of the dislocation. As long as we do not have access to this property, if we assume that long range diffusion fixes PD absorption efficiency, we propose an alternative approach, which consists in relying on the variation of the absorption efficiency with the capture radius, and to extrapolate its value at the dislocation core radius.

Appendix A. Elastic contribution to point-defect formation

In this appendix, we derive the point-defect formation energy at constant volume. We choose to consider the vacancy formation as an example. The self-interstitial atom formation energy can be derived in the same way. We start from system 1 with no vacancy and N atoms A. Hence the volume tensor of the strain-free system is $\underline{V}_1 = N\underline{\Omega}_{at}$, where $\underline{\Omega}_{at} = \Omega_{at}\,\underline{I}/3$ is the atomic volume tensor and $\underline{I}$ is the identity tensor. By this definition, the scalar form of the volume of system 1 is $V_1 = \mathrm{Tr}(\underline{V}_1) = N\Omega_{at}$. We create a vacancy by extracting an atom from the bulk and deposing it at the surface, leading to system 2. System 2 is made of N atoms and 1 vacancy, and thereby has a volume tensor of $\underline{V}_2 = N\underline{\Omega}_{at} + \underline{\Omega}^V_F$, where $\underline{\Omega}^V_F = \underline{\Omega}_{at} + \underline{\Omega}^V_R$ is the so-called formation volume of vacancy, and $\underline{\Omega}^V_R$ is the relaxation volume [i.e., derived from Eq. (15)]. For the sake of simplicity, we assume that the vacancy relaxation volume to be isotropic (which is true in Fe, Ni, and Al)

and $\underline{\Omega}_{\mathrm{R}}^{\mathrm{V}} = \Omega_{\mathrm{R}}^{\mathrm{V}}\,\underline{I}/3$. In this case, the scalar volume of system 2 is $V_2 = \mathrm{Tr}(\underline{V}_2) = N\Omega_{\mathrm{at}} + \Omega_{\mathrm{F}}^{\mathrm{V}}$. We apply to system 2, the strain $\underline{\epsilon}$. In order to compute the vacancy formation energy at fixed volume, we apply a strain $\underline{\epsilon}'$ to system 1 such that there is no change of volume upon the formation of vacancy under the applied strain $\underline{\epsilon}$:

$$V_1\,(\underline{I} + \underline{\epsilon}') = V_2\,(\underline{I} + \underline{\epsilon}). \tag{A.1}$$

Hence,

$$\underline{\epsilon}' = \frac{V_2 - V_1}{V_1}\,\underline{I} + \frac{V_2}{V_1}\,\underline{\epsilon}, \tag{A.2}$$

$$= \frac{\Omega_{\mathrm{F}}^{\mathrm{V}}}{V_1}\,\underline{I} + \left(1 + \frac{\Omega_{\mathrm{F}}^{\mathrm{V}}}{V_1}\right)\underline{\epsilon}. \tag{A.3}$$

The energy of systems 1 and 2 are given by

$$E_1 = NE_{\mathrm{coh}} + \frac{V_1}{2}\,\underline{C}_{ijkl}\,\underline{\epsilon}'_{ij}\,\underline{\epsilon}'_{kl}, \tag{A.4}$$

$$E_2 = NE_{\mathrm{coh}} + E_{\mathrm{V},0}^{\mathrm{F}} + \frac{V_2}{2}\,\underline{C}_{ijkl}\,\underline{\epsilon}_{ij}\,\underline{\epsilon}_{kl}, \tag{A.5}$$

where E_{coh} is the cohesive energy of A, $E_{\mathrm{V},0}^{\mathrm{F}}$ corresponds to the vacancy formation energy in a strain-free system. $\underline{C}$ is the elastic constant fourth-rank tensor. By definition, the vacancy formation energy is equal to $E_{\mathrm{V}}^{\mathrm{F}} = E_2 - E_1$. Hence, we obtain

$$E_{\mathrm{V}}^{\mathrm{F}} = E_{\mathrm{V},0}^{\mathrm{F}} + \frac{V_2}{2}\,\underline{C}_{ijkl}\,\underline{\epsilon}_{ij}\,\underline{\epsilon}_{kl} - \frac{V_1}{2}\,\underline{C}_{ijkl}\,\underline{\epsilon}'_{ij}\,\underline{\epsilon}'_{kl}, \tag{A.6}$$

By relying on Eq. (A.3), we express $\underline{\epsilon}'$ in terms of $\underline{\epsilon}$ and ratio $\Omega_{\mathrm{F}}^{\mathrm{V}}/V_1$. Therefore, we get

$$\begin{aligned} E_{\mathrm{V}}^{\mathrm{F}} = &+ E_{\mathrm{V},0}^{\mathrm{F}} + \frac{V_2}{2}\,\underline{C}_{ijkl}\,\underline{\epsilon}_{ij}\,\underline{\epsilon}_{kl}\,\underline{\epsilon}_{ij} \\ &- \frac{V_1}{2}\left(\frac{\Omega_{\mathrm{F}}^{\mathrm{V}}}{V_1}\right)^2 \underline{C}_{ijkl}\,\underline{I}_{ij}\,\underline{I}_{kl} \\ &- \frac{V_1}{2}\left(\frac{\Omega_{\mathrm{F}}^{\mathrm{V}}}{V_1}\right)\left(1 + \frac{\Omega_{\mathrm{F}}^{\mathrm{V}}}{V_1}\right)\underline{C}_{ijkl}\,\underline{I}_{ij}\,\underline{\epsilon}_{kl} \\ &- \frac{V_1}{2}\left(\frac{\Omega_{\mathrm{F}}^{\mathrm{V}}}{V_1}\right)\left(1 + \frac{\Omega_{\mathrm{F}}^{\mathrm{V}}}{V_1}\right)\underline{C}_{ijkl}\,\underline{\epsilon}_{ij}\,\underline{I}_{kl} \\ &- \frac{V_1}{2}\left(1 + \frac{\Omega_{\mathrm{F}}^{\mathrm{V}}}{V_1}\right)^2 \underline{C}_{ijkl}\,\underline{\epsilon}_{ij}\,\underline{\epsilon}_{kl}. \end{aligned} \tag{A.7}$$

Note that, in the thermodynamic limit, $\Omega_{\mathrm{F}}^{\mathrm{V}}/V_1$ tends to 0. At first order in $\underline{\epsilon}$ and $\Omega_{\mathrm{F}}^{\mathrm{V}}/V_1$, Eq. (A.7) reduces to

$$E_{\mathrm{V}}^{\mathrm{F}} = E_{\mathrm{V},0}^{\mathrm{F}} - \Omega_{\mathrm{F}}^{\mathrm{V}}\,\underline{C}_{iikl}\underline{\epsilon_{kl}}, \tag{A.8}$$

$$= E_{\mathrm{V},0}^{\mathrm{F}} - \Omega_{\mathrm{at}}\,\underline{C}_{iikl}\underline{\epsilon_{kl}} - \underline{P}_{kl}^{\mathrm{sta,V}}\,\underline{\epsilon_{kl}}, \tag{A.9}$$

where $\underline{P}^{\mathrm{sta,V}}$ is the elastic dipole of vacancy V at the stable position and $\underline{P}_{kl}^{\mathrm{sta,V}} = \Omega_{\mathrm{F}}^{\mathrm{V}} \sum_i \underline{C}_{iikl}$. Eq. (A.9) is consistent with Eqs. (6) and (14).

Appendix B. Validation of the simulation approach

In this appendix, we validate our numerical approach by comparing our numerical results to available reference results of the point-defect absorption efficiencies and the bias factor. Analytical expressions of the point-defect absorption efficiencies of a straight edge dislocation are given by Rauh et al. [21] by an exact solution of the diffusion equation. However, there is no exact solution of the dislocation loop bias. An analytical law is provided by Jourdan et al. [31] by fitting the results obtained from finite-element calculation of the elastic bias of an edge dislocation loop. Calculations are performed with the following approximations: (i) the material is perfectly isotropic ($\underline{C}_{44} = (\underline{C}_{11} - \underline{C}_{12})/2$); (ii) PDs are perfectly spherical and isotropic (spherical inclusion approximation); (iii) PDs relaxation energy (elastic dipole contribution) is considered only; (iv) elasto-diffusion is neglected. In order to assess our numerical approach, we solve the diffusion equation using the same approximations and boundary conditions. We set the parameters to the following values : $\underline{C}_{11} = 150\,\mathrm{GPa}$, $\underline{C}_{12} = 50\,\mathrm{GPa}$, $r_{\mathrm{C}} = 2\,b_{\mathrm{v}}$ with the norm of the Burgers vector $b_{\mathrm{v}} = 0.25\,\mathrm{nm}$. The elastic dipole tensors are set to $20\,\underline{I}$ (in eV) for SIAs and $-3\,\underline{I}$ (in eV) for vacancies, with $\underline{I}$ the identity tensor. The comparison between our results and the reference ones are plotted in Figs. B.13 and B.14. Our numerical solutions are in excellent agreement with the reference results (the relative difference is within $\pm 1\%$ with the reference solutions from Ref. [21] for the straight dislocation and $\pm 4\%$ for the dislocation loop with the fitted law in Ref. [31]).

Acknowledgments

Dr. Emmanuel Clouet and Dr. Thomas Jourdan are acknowledged for fruitful discussions on the elastic contribution to the diffusion driving force, with a special thank to Dr. Emmanuel Clouet for the calculation of the formation free energy in the (NVT) ensemble. Aix-Marseille mesocentre and CPPM computing department are acknowledged for granting access to their high-performance computing resources.

Data availability

The authors confirms that the data supporting the findings of this study are available within the article. Raw data that support the findings of this study are available from the corresponding author, upon reasonable request.

References

[1] J. P. Hirth, J. Lothe, T. Mura, Theory of Dislocations (2nd ed.), J. Appl. Mech. 50 (2) (1983) 476–477. doi:10.1115/1.3167075. URL https://asmedigitalcollection.asme.org/appliedmechanics/article/50/2/476/389516/Theory-of-Dislocations-2nd-ed

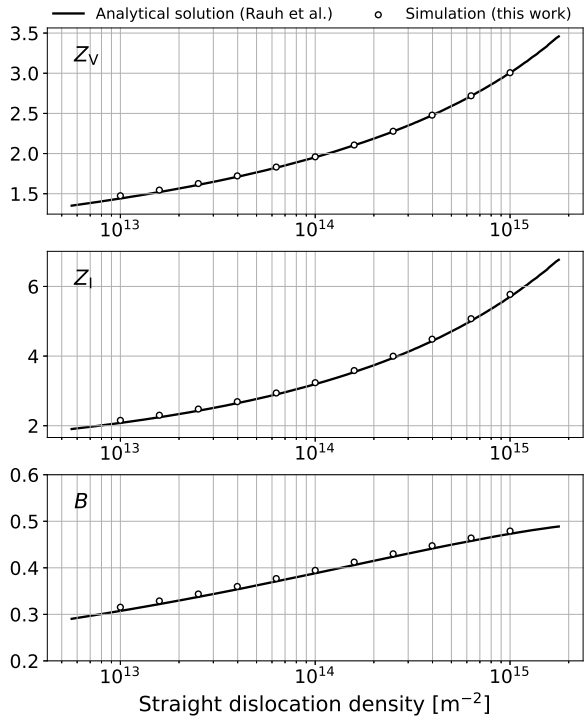

Figure B.13: PD absorption efficiency and elastic bias of a straight edge dislocation in function of the dislocation density. The solid line is obtained from the analytical solution in Ref. [21]. The unfilled symbols are our calculations.

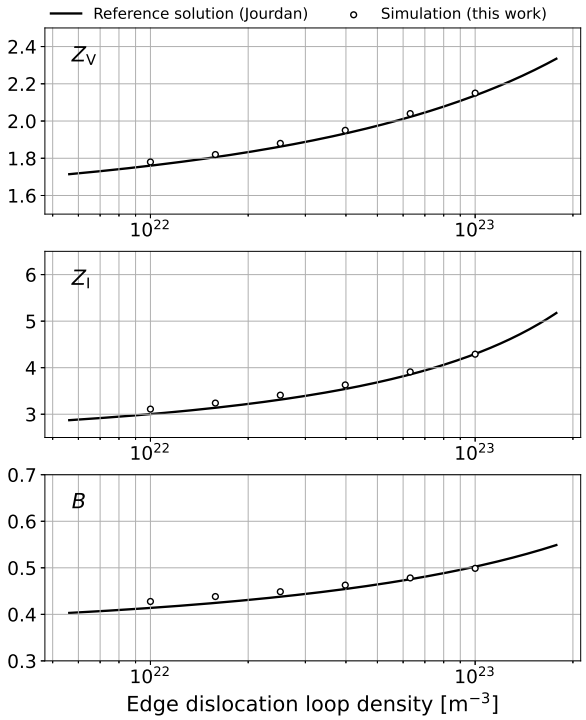

Figure B.14: PD absorption efficiency and elastic bias of a straight edge dislocation in function of the dislocation density. The solid line is obtained from the analytical solution in Ref. [31]. The unfilled symbols are our calculations.

[2] C. Varvenne, F. Bruneval, M.-C. Marinica, E. Clouet, Point defect modeling in materials: Coupling ab initio and elasticity approaches, Physical Review B 88 (13) (2013) 134102. doi:10.1103/PhysRevB.88.134102.
URL https://link.aps.org/doi/10.1103/PhysRevB.88.134102

[3] E. Clouet, C. Varvenne, T. Jourdan, Elastic modeling of point-defects and their interaction, Comput. Mater. Sci. 147 (2018) 49–63. arXiv:1802.04062, doi:10.1016/j.commatsci.2018.01.053.
URL https://doi.org/10.1016/j.commatsci.2018.01.053

[4] J. Lothe, J. P. Hirth, Dislocation Climb Forces, J. Appl. Phys. 38 (2) (1967) 845–848. doi:10.1063/1.1709423.
URL http://aip.scitation.org/doi/10.1063/1.1709423

[5] G. W. Greenwood, A. J. Foreman, D. E. Rimmer, The role of vacancies and dislocations in the nucleation and growth of gas bubbles in irradiated fissile material, J. Nucl. Mater. 1 (4) (1959) 305–324. doi:10.1016/0022-3115(59)90030-3.

[6] C. CAWTHORNE, E. J. FULTON, Voids in Irradiated Stainless Steel, Nature 216 (5115) (1967) 575–576. doi:10.1038/216575a0.
URL http://www.nature.com/articles/216575a0

[7] A. D. Brailsford, R. Bullough, The rate theory of swelling due to void growth in irradiated metals, J. Nucl. Mater. 44 (2) (1972) 121–135. doi:10.1016/0022-3115(72)90091-8.

[8] P. T. Heald, M. V. Speight, Point defect behaviour in irradiated materials, Acta Metall. 23 (11) (1975) 1389–1399. doi:10.1016/0001-6160(75)90148-0.

[9] T. Okita, W. Wolfer, A critical test of the classical rate theory for void swelling, Journal of Nuclear Materials 327 (2-3) (2004) 130–139. doi:10.1016/j.jnucmat.2004.01.026.
URL https://linkinghub.elsevier.com/retrieve/pii/S0022311504000765

[10] D. Carpentier, T. Jourdan, Y. Le Bouar, M. C. Marinica, Effect of saddle point anisotropy of point defects on their absorption by dislocations and cavities, Acta Mater. 136 (2017) 323–334. doi:10.1016/j.actamat.2017.07.013.
URL http://dx.doi.org/10.1016/j.actamat.2017.07.013

[11] G. F. Bouobda Moladje, L. Thuinet, C. Domain, C. S. Becquart, A. Legris, Phase-field calculations of sink strength in Al, Ni, and Fe: A detailed study of elastic effects, Computational Materials Science 183 (June) (2020). doi:10.1016/j.commatsci.2020.109905.

[12] J. Weertman, The Peach–Koehler equation for the force on a dislocation modified for hydrostatic pressure, Philos. Mag. A J. Theor. Exp. Appl. Phys. 11 (114) (1965) 1217–1223. doi:10.1080/14786436508224930.
URL https://www.tandfonline.com/doi/full/10.1080/14786436508224930

[13] P. H. Dederichs, K. Schroeder, Anisotropic diffusion in stress fields, Physical Review B 17 (6) (1978) 2524–2536. doi:10.1103/PhysRevB.17.2524.
URL https://link.aps.org/doi/10.1103/PhysRevB.17.2524

[14] L. Onsager, RECIPROCAL RELATIONS IN IRREVERSIBLE PROCESSES. I., Phys. Rev. 37 (1931) 405–426. doi:10.1103/PhysRev.37.405.

[15] A. R. Allnatt, A. B. Lidiard, Atomic Transport in Solids, Cambridge University Press, 1993.

[16] L. Onsager, RECIPROCAL RELATIONS IN IRREVERSIBLE PROCESSES. II., Phys. Rev. 38 (1931) 2265–2279. doi:10.1103/PhysRev.38.2265.

[17] D. R. Trinkle, Diffusivity and derivatives for interstitial solutes: activation energy, volume, and elastodiffusion tensors, Philos. Mag. 96 (26) (2016) 2714–2735. doi:10.1080/14786435.2016.1212175.
URL http://dx.doi.org/10.1080/14786435.2016.1212175https://www.tandfonline.com/doi/full/10.1080/14786435.2016.1212175

[18] D. L. Olmsted, R. Phillips, W. A. Curtin, Modelling diffusion in crystals under high internal stress gradients, Modelling and Simulation in Materials Science and Engineering 12 (5) (2004) 781–797. doi:10.1088/0965-0393/12/5/003.
URL https://doi.org/10.1088/0965-0393/12/5/003

[19] W. Wolfer, Fundamental Properties of Defects in Metals, in: Compr. Nucl. Mater., Vol. 1, Elsevier, 2012, pp. 1–45. doi:10.1016/B978-0-08-056033-5.00001-X.
URL http://dx.doi.org/10.1016/B978-0-08-056033-5.00001-Xhttps://linkinghub.elsevier.com/retrieve/pii/B978008056033500001X

[20] D. Carpentier, Simulation of absorption kinetics of point defects by dislocations and defect clusters, Theses, Université Paris-Saclay (Oct. 2018).
URL https://pastel.archives-ouvertes.fr/tel-01915303

[21] H. Rauh, D. Simon, On the diffusion process of point defects in the stress field of edge dislocations, Phys. Status Solidi 46 (2) (1978) 499–510. doi:10.1002/pssa.2210460213.

[22] T. Garnier, V. R. Manga, D. R. Trinkle, M. Nastar, P. Bellon, Stress-induced anisotropic diffusion in alloys: Complex Si solute flow near a dislocation core in Ni, Phys. Rev. B 88 (13) (2013) 134108. doi:10.1103/PhysRevB.88.134108.
URL https://link.aps.org/doi/10.1103/PhysRevB.88.134108

[23] Z. Li, D. R. Trinkle, Mesoscale modeling of vacancy-mediated Si segregation near an edge dislocation in Ni under irradiation, Phys. Rev. B 95 (14) (2017) 144107. doi:10.1103/PhysRevB.95.144107.
URL http://link.aps.org/doi/10.1103/PhysRevB.95.144107

[24] T. Schuler, L. Messina, M. Nastar, KineCluE: A kinetic cluster expansion code to compute transport coefficients beyond the dilute limit, Comput. Mater. Sci. 172 (May 2019) (2020) 109191. doi:10.1016/j.commatsci.2019.109191.
URL https://doi.org/10.1016/j.commatsci.2019.109191https://linkinghub.elsevier.com/retrieve/pii/S0927025619304902

[25] E. Clouet, Predicting dislocation climb: Classical modeling versus atomistic simulations, Physical Review B 84 (9) (2011) 092106. doi:10.1103/PhysRevB.84.092106.
URL https://link.aps.org/doi/10.1103/PhysRevB.84.092106

[26] C. Woo, W. Liu, M. Wuschke, A finite-difference calculation of point defect migration into a dislocation loop (1979).
URL https://inis.iaea.org/search/search.aspx?orig_q=RN:11558103

[27] R. Bullough, M. Wood, D. Wells, J. Willis, THE INTERACTION ENERGY BETWEEN INTERSTITIAL ATOMS AND DISLOCATIONS AND ITS RELEVANCE TO IRRADIATION DAMAGE PROCESSES, in: Dislocation Modelling of Physical Systems, Elsevier, 1981, pp. 116–141. doi:10.1016/B978-0-08-026724-1.50017-0.
URL https://linkinghub.elsevier.com/retrieve/pii/B9780080267241500170

[28] W. Coghlan, M. Yoo, RADIUS DEPENDENCE OF THE SINK STRENGTH OF A DISLOCATION LOOP, in: Dislocation Modelling of Physical Systems, Elsevier, 1981, pp. 152–157. doi:10.1016/B978-0-08-026724-1.50020-0.
URL https://linkinghub.elsevier.com/retrieve/pii/B9780080267241500200

[29] V. I. Dubinko, A. S. Abyzov, A. A. Turkin, Numerical evaluation of the dislocation loop bias, J. Nucl. Mater. 336 (1) (2005) 11–21. doi:10.1016/j.jnucmat.2004.07.034.

[30] W. G. Wolfer, The Dislocation Bias, Journal of Computer-Aided Materials Design 14 (3) (2007) 403–417. doi:10.1007/s10820-007-9051-3.
URL http://link.springer.com/10.1007/s10820-007-9051-3

[31] T. Jourdan, Influence of dislocation and dislocation loop biases on microstructures simulated by rate equation cluster dynamics, J. Nucl. Mater. 467 (2015) 286–301. doi:10.1016/j.jnucmat.2015.09.046.
URL http://dx.doi.org/10.1016/j.jnucmat.2015.09.046

[32] F. A. Nichols, On the estimation of sink-absorption terms in reaction-rate-theory analysis of radiation damage, J. Nucl. Mater. 75 (1) (1978) 32–41. doi:10.1016/0022-3115(78)90026-0.

[33] R. Chang, The dilatational strain field associated with edge dislocations and edge dislocation walls based on anisotropic elasticity, Acta Metall. 10 (10) (1962) 951–958. doi:10.1016/0001-6160(62)90145-1.
URL https://linkinghub.elsevier.com/retrieve/pii/0001616062901451

[34] Z. Chang, P. Olsson, D. Terentyev, N. Sandberg, Dislocation bias factors in fcc copper derived from atomistic calculations, J. Nucl. Mater. 441 (1-3) (2013) 357–363. doi:10.1016/j.jnucmat.2013.06.029.
URL http://dx.doi.org/10.1016/j.jnucmat.2013.06.029

[35] A. Seeger, U. Gösele, Steady-state diffusion of point defects to dislocation loops, Phys. Lett. A 61 (6) (1977) 423–425. doi:10.1016/0375-9601(77)90355-3.

[36] L. Messina, M. Nastar, T. Garnier, C. Domain, P. Olsson, Exact ab initio transport coefficients in bcc Fe–X (X = Cr, Cu, Mn, Ni, P, Si) dilute alloys, Phys. Rev. B 90 (10) (2014) 104203. doi:10.1103/PhysRevB.90.104203.
URL https://link.aps.org/doi/10.1103/PhysRevB.90.104203

[37] J. D. Tucker, R. Najafabadi, T. R. Allen, D. Morgan, Ab initio-based diffusion theory and tracer diffusion in Ni-Cr and Ni-Fe alloys, J. Nucl. Mater. 405 (3) (2010) 216–234. doi:10.1016/j.jnucmat.2010.08.003.
URL http://dx.doi.org/10.1016/j.jnucmat.2010.08.003

[38] M. I. Mendelev, S. Han, D. J. Srolovitz, G. J. Ackland, D. Y. Sun, M. Asta, Development of new interatomic potentials appropriate for crystalline and liquid iron, Philosophical Magazine 83 (35) (2003) 3977–3994. doi:10.1080/14786430310001613264.
URL http://www.tandfonline.com/doi/abs/10.1080/14786430310001613264

[39] C. Kittel, Introduction to solid state physics, 8th Edition, John Wiley & Sons, New York, NY, 2004.

[40] L. Messina, T. Schuler, M. Nastar, M.-C. Marinica, P. Olsson, Solute diffusion by self-interstitial defects and radiation-induced segregation in ferritic Fe–X (X=Cr, Cu, Mn, Ni, P, Si) dilute alloys, Acta Materialia 191 (2020) 166–185. doi:10.1016/j.actamat.2020.03.038.
URL https://linkinghub.elsevier.com/retrieve/pii/S1359645420302251

[41] C. Gordon, A. Granato, Equilibrium concentration of interstitials in aluminum just below the melting temperature, Materials Science and Engineering: A 370 (1-2) (2004) 83–87. doi:10.1016/j.msea.2003.08.077.
URL https://linkinghub.elsevier.com/retrieve/pii/S0921509303008414

[42] L. A. Girifalco, Diffusion in non-uniform crystals, Materials Science and Engineering 9 (C) (1972) 61–79. doi:10.1016/0025-5416(72)90018-3.

[43] W. G. Wolfer, M. Ashkin, Diffusion of vacancies and interstitials to edge dislocations, Journal of Applied Physics 47 (3) (1976) 791–800. doi:10.1063/1.322710.
URL http://aip.scitation.org/doi/10.1063/1.322710

[44] D. Seif, N. M. Ghoniem, Effect of anisotropy, SIA orientation, and one-dimensional migration mechanisms on dislocation bias calculations in metals, Journal of Nuclear Materials 442 (1-3) (2013) S633–S638. doi:10.1016/j.jnucmat.2013.02.083.
URL http://dx.doi.org/10.1016/j.jnucmat.2013.02.083https://linkinghub.elsevier.com/retrieve/pii/S0022311513005382

[45] Z. Chang, N. Sandberg, D. Terentyev, K. Samuelsson, G. Bonny, P. Olsson, Assessment of the dislocation bias in fcc metals and extrapolation to austenitic steels, J. Nucl. Mater. 465 (2015) 13–19. doi:10.1016/j.jnucmat.2015.05.042.

[46] J. Hirth (Ed.), Theory of Dislocations, 2nd Edition, Wiley, New

York, 1982.

[47] D. Mordehai, E. Clouet, M. Fivel, M. Verdier, Introducing dislocation climb by bulk diffusion in discrete dislocation dynamics, Philosophical Magazine 88 (6) (2008) 899–925. doi:10.1080/14786430801992850.
URL http://www.tandfonline.com/doi/abs/10.1080/14786430801992850

[48] B. Bakó, E. Clouet, L. M. Dupuy, M. Blétry, Dislocation dynamics simulations with climb: kinetics of dislocation loop coarsening controlled by bulk diffusion, Philosophical Magazine 91 (23) (2011) 3173–3191. doi:10.1080/14786435.2011.573815.
URL http://www.tandfonline.com/doi/abs/10.1080/14786435.2011.573815

[49] D. Mordehai, G. Martin, Enhanced annealing of the dislocation network under irradiation, Physical Review B 84 (1) (2011) 014115. doi:10.1103/PhysRevB.84.014115.
URL https://link.aps.org/doi/10.1103/PhysRevB.84.014115

[50] M. Kabir, T. T. Lau, D. Rodney, S. Yip, K. J. Van Vliet, Predicting Dislocation Climb and Creep from Explicit Atomistic Details, Physical Review Letters 105 (9) (2010) 095501. doi:10.1103/PhysRevLett.105.095501.
URL https://link.aps.org/doi/10.1103/PhysRevLett.105.095501

[51] M. Nastar, F. Soisson, Radiation-induced segregation, Vol. 1, Elsevier Inc., 2020. doi:10.1016/B978-0-12-803581-8.00668-8.
URL http://dx.doi.org/10.1016/B978-0-12-803581-8.00668-8